



Cite this: *Chem. Commun.*, 2017, 53, 20

# Beyond methylammonium lead iodide: prospects for the emergent field of $ns^2$ containing solar absorbers

Alex M. Ganose,<sup>†ab</sup> Christopher N. Savory<sup>†a</sup> and David O. Scanlon<sup>\*ab</sup>

The field of photovoltaics is undergoing a surge of interest following the recent discovery of the lead hybrid perovskites as a remarkably efficient class of solar absorber. Of these, methylammonium lead iodide (MAPI) has garnered significant attention due to its record breaking efficiencies, however, there are growing concerns surrounding its long-term stability. Many of the excellent properties seen in hybrid perovskites are thought to derive from the  $6s^2$  electronic configuration of lead, a configuration seen in a range of post-transition metal compounds. In this review we look beyond MAPI to other  $ns^2$  solar absorbers, with the aim of identifying those materials likely to achieve high efficiencies. The ideal properties essential to produce highly efficient solar cells are discussed and used as a framework to assess the broad range of compounds this field encompasses. Bringing together the lessons learned from this wide-ranging collection of materials will be essential as attention turns toward producing the next generation of solar absorbers.

Received 5th August 2016,  
Accepted 29th September 2016

DOI: 10.1039/c6cc06475b

www.rsc.org/chemcomm

## 1 Introduction

As modern society continues to consume natural resources at an ever-increasing rate, there is a growing demand for a clean energy source capable of providing indefinite and sustainable

economic growth.<sup>1</sup> Arguably the most abundant renewable energy resource is sunlight, with over 1500 exawatt-hours of energy falling incident on the earth in the form of solar radiation each year.<sup>2</sup> The enormity of this resource is apparent when one considers that the total known reserves of oil, gas and coal amount to just 9 exawatt-hours. A year's worth of sunlight, therefore, provides almost two hundred times the energy of the world's entire known supply of fossil fuels.<sup>3</sup> Of the technologies available to harness solar radiation, photovoltaic cells are perhaps the most promising due to their ability to convert light directly into electricity. Indeed, coverage of less than 0.3% of the earth's surface would be sufficient to meet the world's

<sup>a</sup> University College London, Kathleen Lonsdale Materials Chemistry, Department of Chemistry, 20 Gordon Street, London WC1H 0AJ, UK. E-mail: d.scanlon@ucl.ac.uk; Tel: +44 (0)1234 567 890

<sup>b</sup> Diamond Light Source Ltd., Diamond House, Harwell Science and Innovation Campus, Didcot, Oxfordshire OX11 0DE, UK

<sup>†</sup> These authors contributed equally to this work.



Alex M. Ganose

Alex Ganose received his MSci (2014) in Natural Sciences and MRes (2015) in Molecular Modelling and Materials Science from University College London, UK. He is currently studying towards his EngD in Molecular Modelling and Materials Science under Dr David Scanlon at University College London. His research is focused on the computational design of earth-abundant and non-toxic solar absorbers.



Christopher N. Savory

Chris Savory received his MChem degree from the University of Oxford in 2014. He is now working towards his PhD in Inorganic Chemistry under the supervision of Dr David Scanlon at University College London. His research interests include the *ab initio* computational investigation of hybrid inorganic-organic, silver and bismuth materials for photovoltaic and other renewable energy applications.



energy needs using the latest commercially available solar panels. However, in order for photovoltaic cells to compete with fossil fuels in utility-scale power generation, it is necessary to reduce the total cost of solar energy, either through increased efficiencies or lower cost per photovoltaic cell.<sup>4</sup>

The current photovoltaic market is dominated by crystalline silicon solar cells, which, having benefited from six decades of research, possess power conversion efficiencies (PCEs) around 21%.<sup>5</sup> However, the performance of these cells is limited by the indirect band gap of silicon and the last five years have seen little improvement to their efficiencies. Currently, the highest performing single-junction solar cells are those containing GaAs. These devices have shown efficiencies approaching the Shockley–Queisser limit of 33%<sup>6</sup> but due to the high raw materials cost of GaAs (~7 times that of crystalline silicon),<sup>7</sup> their viability is limited to extraterrestrial applications where efficiency presides over cost.<sup>8</sup>

Recently, hybrid halide perovskite solar cells have emerged as a serious contender to silicon-based devices thanks to an unprecedented rise in efficiency—reaching 22% in 2016, overtaking all other third-generation technologies.<sup>9,10</sup> CH<sub>3</sub>NH<sub>3</sub>PbI<sub>3</sub> (MAPI) is the champion hybrid halide perovskite absorber and has, as such, attracted an enormous volume of research interest. MAPI possesses many of the ideal properties for a solar absorber: a direct band gap of 1.55 eV,<sup>11</sup> small exciton binding energies,<sup>12</sup> high levels of defect self-regulation,<sup>13</sup> remarkably long charge carrier diffusion lengths,<sup>14,15</sup> and excellent charge carrier mobilities.<sup>16–18</sup> It can also be solution-processed allowing for low-cost fabrication and has been shown to perform well with a wide range of hole and electron contact materials, allowing for widespread application.<sup>19–21</sup> However, the intrinsic long-term stability of the MAPI structure is poor<sup>22,23</sup> and, despite considerable effort, remains a significant challenge facing the hybrid perovskite community.<sup>24–26</sup>

Many studies have tried to bypass the instability of MAPI by exploring alternative compounds within the perovskite composition space.<sup>27–29</sup> However, attempts to replace methylammonium with other organic and inorganic cations outside of those already known in the literature has proved exceedingly challenging.<sup>30,31</sup> Whilst the tolerance factor metric has traditionally been applied as a predictor of perovskite stability, it performs poorly across the range of known iodide perovskites.<sup>32,33</sup> Recently, a revised tolerance factor method has been developed that takes into account the greater covalency seen in some metal–halide bonds and is able to accurately predict the stability of the majority of halide perovskites.<sup>34</sup> Strikingly, the report suggests that only a handful of halide perovskites remain to be discovered, with most likely to possess band gaps unsuitable for photovoltaic applications. It is therefore essential, now more than ever, that the search for the next generation of solar absorbers be extended beyond the cubic perovskite motif.

The meteoric rise in the efficiency of MAPI has fuelled intense interest among a broad community of physicists, chemists, and engineers and has brought together the lessons learned in over 20 years of development of related dye-sensitised and organic photovoltaic cells.<sup>35,36</sup> Brandt *et al.* have recently proposed several key properties likely to give rise to highly efficient and defect-tolerant solar absorbers, including a large dielectric constant, small effective masses, a valence band maximum composed of antibonding states, and high levels of band dispersion.<sup>37</sup> Materials containing post-transition metals with an *ns*<sup>2</sup> electronic configuration (*i.e.* an N-2 oxidation state) possess many of these properties due to their soft polarisability—leading to high Born effective charges—and large spin-orbit effects, which act to increase the bandwidth of the conduction band.<sup>38,39</sup> As such, a wide range of compounds comprising Pb<sup>2+</sup>, Sn<sup>2+</sup>, Ge<sup>2+</sup>, Sb<sup>3+</sup>, and Bi<sup>3+</sup> cations are currently of interest for their solar absorber ability.

In this Review we focus on this emerging field of *ns*<sup>2</sup> containing solar absorbers. The ideal properties needed to produce highly efficient solar cells are discussed and used as a framework to assess the broad range of compounds this field encompasses. Initially, group 14-based materials—those containing lead, tin and germanium—are examined, with both well established and novel absorbers considered. The second half of this Review concerns materials containing the group 15 post-transition metals antimony and bismuth. Throughout, particular attention is given to the relationship between structure and properties, specifically the effect of dimensionality on stability and carrier transport. Lastly, we look towards the future of next generation solar absorbers.

## 2 Desired solar absorber properties

The performance of novel solar absorbers is hard to predict in practice, due to the dependence on many external conditions such as the method of deposition, quality of precursor and device architecture. However, analysis of high performance solar materials reveals several key properties likely to beneficially



**David O. Scanlon**

*David O. Scanlon received his degree in Computational Chemistry (2006) and PhD in Chemistry (2011) from Trinity College Dublin, Ireland. After a Ramsay Fellowship in the Department of Chemistry at UCL, he was appointed to a Lectureship (2013) and then as a Reader (2016) in Computational, Inorganic and Materials Chemistry at UCL and at Diamond Light Source. He currently leads the Materials Theory Group, which focusses on*

*the use of Computational Chemistry techniques to understand and predict the behaviours of solid state materials, primarily for renewable energy applications. The group is currently working on novel materials for photovoltaics and photocatalysis, Li-ion batteries, thermoelectrics, and optimising materials for thin film displays.*



affect device efficiencies.<sup>37</sup> Crucially, many of these properties, whilst difficult to measure experimentally, can be obtained relatively cheaply from theoretical methods, thus highlighting the importance of a combined theoretical/experimental approach in screening new materials.

## 2.1 Magnitude and nature of the band gap

Arguably the most important property of a solar absorber is its band gap, as it determines the maximum theoretical PCE possible for the material. The best performing absorbers possess band gaps in the 1.10–1.55 eV range, as quantified by the well-known Shockley–Queisser limit,<sup>6</sup> which takes into account the antagonistic dependence of short-circuit current ( $J_{sc}$ ) and open-circuit voltage ( $V_{oc}$ ) on the band gap and solar spectrum (Fig. 1a). While this does not preclude materials with band gaps outside this range being examined, in order to maximise efficiency, a band gap close to 1.3 eV is highly advantageous.

## 2.2 Strength of optical absorption

Strong optical absorption is particularly crucial for solar absorbers: many compounds with ideal band gaps are poor absorbers. Indeed, low absorbance due to an indirect band gap is one of the primary reasons to look beyond crystalline silicon as an absorber. As recently stressed by Yu and Zunger, strong absorption requires a direct band gap transition; however, materials

with indirect band gaps may still perform well if a direct transition of suitable energy is also available.<sup>40</sup> Loss in absorption can further result if the fundamental band gap is dipole disallowed, widening the optical band gap relative to the fundamental gap, as often results in centrosymmetric materials.<sup>41,42</sup> Ideally, strong absorption is characterised by a steep absorption edge in the absorption coefficient,  $\alpha$ , just above the band gap, up to  $10^4$ – $10^5$  cm<sup>-1</sup> or higher (Fig. 1b).<sup>43</sup>

## 2.3 Charge carrier effective mass

High charge carrier mobilities can be particularly useful in photovoltaics for establishing electron–hole separation and improving device performance. Mobility,  $\mu$ , is dependent on the dispersion of the band edges in a material—theoretically quantified by the effective mass of a carrier—with greater dispersion giving rise to smaller effective masses and in turn, enhanced carrier mobilities (Fig. 1c). The primary limiter of carrier mobility is through scattering by defects, phonons and other charge carriers. We note that mobility is not the only important transport property: minority-carrier lifetimes,  $\tau$ , have recently been proposed as an essential metric for screening novel PV materials, due to their role in Shockley–Read–Hall recombination (trap-assisted non-radiative recombination).<sup>37,46,47</sup> Indeed, MAPI's excellent performance is dependent on both



**Fig. 1** Desired solar absorber properties: (a) ideal range of solar absorber band gaps (shaded) projected onto the AM1.5 solar spectrum (yellow) and the Shockley–Queisser limit (blue); (b) importance of a direct band gap transition—crystalline silicon (c-Si, purple) has dramatically weaker absorption relative to GaAs (green) and MAPI (red); (c) schematic band structure indicating how greater band dispersion (curvature) gives rise to smaller hole and electron effective masses; (d) the impact of bonding structure on defect tolerance, with antibonding states at the top of the valence band maximum giving rise to shallower defects; (e) schematic of absorption and recombination processes in Rashba spin-split systems; (f) band alignment in a heterojunction solar cell. Efficient alignment between materials results in a larger maximum obtainable open circuit voltage ( $V_{oc}$ ). The Fermi level of the n-type transparent conducting oxide (TCO) and p-type hole transporting material (HTM) layers is denoted by  $E_{F,n}$  and  $E_{F,p}$ , respectively. In panels (c) and (e) conduction bands and valence bands are shown in orange and blue, respectively; (b), (d), and (e) adapted with permission from ref. 43–45.



its high mobilities and very long carrier lifetimes and diffusion lengths.<sup>17,48</sup>

## 2.4 Defect tolerance

Defect tolerance is the ability for semiconductors to retain strong optoelectronic properties, particularly power conversion efficiency, regardless of the presence of defects, including point defects and grain boundaries.<sup>49</sup> One of the proposed mechanisms by which defect tolerance may occur is the presence of antibonding interactions at the valence band maximum (Fig. 1d)—as a result, defects are confined to shallow states at the band edges, rather than deep gap states that may act as traps and recombination centres.<sup>44</sup> As Brandt *et al.* recently highlighted, ions such as Sn<sup>2+</sup> and Bi<sup>3+</sup> are highly likely to have this bonding composition due to the active *ns*<sup>2</sup> lone pair, and so present excellent candidates for defect tolerant compounds.<sup>37</sup>

## 2.5 Dielectric constant and ferroelectric behaviour

Electric response can also be vital to a photovoltaic absorber. A large static dielectric constant has perhaps the most obvious benefit, particularly with regard to some of the aforementioned properties—it confers a high degree of charge screening, resulting in smaller defect charge-capture cross-sections, and inhibits radiative electron-hole recombination. Furthermore, for ‘hydrogenic’ defects, a large dielectric constant enables smaller defect binding energies promoting shallower defect states.<sup>50</sup> As with defect tolerance, large highly polarizable cations like Pb<sup>2+</sup> are likely to lead to high dielectric properties. Ferroelectric behaviour has also been of considerable interest with regards to MAPI’s hysteresis;<sup>38,51,52</sup> while current evidence suggests it may not be the primary cause of hysteresis,<sup>53</sup> the prospect of useable photo-ferroic devices, and high photovoltages from the anomalous photovoltaic effect, remains enticing.<sup>16,54</sup>

## 2.6 Rashba splitting

‘Spintronics’ is an emergent field in condensed matter physics, of which MAPI has seen its share of interest. Recently, Rashba splitting in the MAPI electronic band structure has been implicated in strongly reducing radiative recombination and is considered a possible cause of its high carrier lifetimes.<sup>55,56</sup> Indeed, the spin-split indirect gap seen in MAPI is thought to reduce the recombination rate by a factor of more than 350% compared to direct band gap behaviour (Fig. 1e).<sup>45</sup> Non-centrosymmetric structures with heavy elements such as bismuth and lead could easily demonstrate similar effects due to their strong spin orbit coupling. Likewise, multivalley band structures are also thought to increase charge carrier mobilities through separation of charge carriers, in addition to ensuring a high density of states at the band edges, leading to higher absorption coefficients.<sup>40,57</sup>

## 2.7 Alignment with commonly used contact materials

During heterojunction cell construction, care must be taken to ensure close band alignment of the absorber with its neighbouring materials, such as buffer layers and contacts materials. Efficient band alignment prevents loss of  $V_{oc}$  and enables facile

carrier transport throughout the cell (Fig. 1f). While layers can be tuned to ensure this, an absorber with typical band positions that align well with ubiquitous components like F-doped SnO<sub>2</sub> would be highly advantageous to reducing the cost and difficulty of manufacture and distribution.

# 3 Lead absorbers

## 3.1 Perovskite structured

As previously mentioned, stability is a major concern limiting the use of hybrid halide perovskites in commercial photovoltaic devices, primarily as longevity is crucial to reach energy payback times.<sup>58</sup> Many studies have focused on moisture degradation of MAPI cells,<sup>59,60</sup> highlighting the facile hydrolysis of the absorbing layer upon contact with air.<sup>61–63</sup> Additionally, MAPI possesses poor thermal stability and is known to rapidly decompose at temperatures above 85 °C,<sup>64,65</sup> with research indicating that the MAPI structure is intrinsically unstable with respect to phase separation into CH<sub>3</sub>NH<sub>3</sub>PbI<sub>3</sub> and PbI<sub>2</sub>.<sup>25,66</sup> This instability has recently been attributed, with the aid of computational studies, to the low formation energy of MAPI.<sup>67,68</sup> As such, modifications of the MAPI formula that are able to increase stability have become highly desirable.<sup>69</sup>

One method of tuning MAPI’s electronic properties is through changing the organic cation (Fig. 2a). So far, only methylammonium (MA) and formamidinium (FA) have been successfully incorporated into the perovskite structure, with larger cations resulting in lower dimensionality structures due to disruption of the three-dimensional (3D) Pb–I cage.<sup>31,70,71</sup> Replacing MA with FA to yield CH(NH<sub>2</sub>)<sub>2</sub>PbI<sub>3</sub> (FAPbI<sub>3</sub>), results in films with a slightly smaller band gap of 1.48 eV, long photoluminescence (PL) lifetimes, lower rates of recombination, high PCEs, and enhanced thermal stability.<sup>72,73</sup> Unfortunately, the synthesis of FAPbI<sub>3</sub> is complicated by the formation of a thermally accessible hexagonal  $\delta$ -phase, whose large band gap adversely affects device performance.<sup>74,75</sup> FAPbI<sub>3</sub> films incorporating up to 20% MA show considerable stabilisation of the black  $\alpha$ -phase during synthesis and possess long exciton lifetimes and high efficiencies,<sup>76,77</sup> however, the long term stability of these films has not yet been addressed. Alternatively, replacing the organic component of MAPI with an inorganic cation to produce an all-inorganic perovskite is considered a possible route to enhanced stabilities.<sup>78,79</sup> Eperon *et al.* have recently demonstrated a working CsPbI<sub>3</sub> based device by preventing the formation of the weakly absorbing yellow non-perovskite phase.<sup>80,81</sup> Their cells showed remarkable thermal stability up to 300 °C but possessed poor efficiencies of only 2.9% and extreme sensitivity to ambient conditions.

MAPI can also be tuned through the replacement of iodide with other halides (Fig. 2a).<sup>82</sup> In many early cells, using a PbCl<sub>2</sub> precursor incorporated a very small proportion of the chlorine, leading to improved film morphologies due to better distributed heterogeneous nucleation.<sup>48,83,84</sup> On the other hand, inclusion of bromide in a solid solution, allows for a tunable band gap<sup>85</sup> and lower levels of hysteresis.<sup>86</sup> Based on this Rehman *et al.* evaluated





**Fig. 2** (a) Schematic of perovskite structure indicating the A, B, and X lattice sites. Reprinted with permission from ref. 90. Copyright 2015, American Chemical Society. (b–d) Photographs (b), ultraviolet-visible absorbance spectra (c) and X-ray diffraction patterns (d) of  $\text{FAPbI}_{1-x}\text{Br}_x$  and  $\text{FA}_{0.83}\text{Cs}_{0.17}\text{PbI}_{1-x}\text{Br}_x$  perovskite films, with Br composition increasing from  $x = 0$  to 1. From ref. 89. Reprinted with permission from AAAS. (e) Layered (100)-oriented perovskite structures, where  $n = \infty$  denotes the cubic 3D perovskite,  $n = 1$  corresponds to the 2D layered structure, and  $n > 1$  describes “quasi-2D” structures. Reprinted with permission from ref. 70. (f) Crystal structure and (g) piezochromic response of  $(\text{CH}_3\text{NH}_3)_2\text{Pb}(\text{SCN})_2$  (MAPSI). Reprinted with permission from ref. 91. Copyright 2016, American Chemical Society.

the mixed Br/I system,  $\text{FAPb}(\text{Br}_x\text{I}_{1-x})_3$ , for use in tandem solar cells.<sup>87</sup> It was noted that the composition needed to form an ideal top-cell band gap of  $\sim 1.7\text{--}1.8$  eV (namely  $x = 0.3\text{--}0.5$ ), resulted in apparently “amorphous” phases with reduced charge-carrier diffusion lengths, high levels of energetic disorder, and poor optical absorption. This is also observed in theoretical calculations of the  $\text{MAPb}(\text{Br}_x\text{I}_{1-x})_3$  system, in which the region between  $0.3 < x < 0.6$  is unstable with respect to spinodal decomposition at 300 K.<sup>88</sup> Recently, McMeekin *et al.* have demonstrated a mixed-cation mixed-halide perovskite system, in which the phase instability region is subjugated through partial substitution of FA with Cs (Fig. 2b–d).<sup>89</sup> The resulting thin films, with the composition  $\text{FA}_{0.83}\text{Cs}_{0.17}\text{Pb}(\text{I}_{0.6}\text{Br}_{0.4})_3$ , possessed excellent crystallinity, an optical band gap of 1.74 eV, a high open circuit voltage ( $V_{\text{OC}}$ ) of 1.2 eV and efficiencies competitive with those seen in MAPI based solar cells (up to 17.9%). The same composition was employed as a semitransparent cell along with a crystalline silicon module, in order to assess the potential of these films for tandem architectures, with an efficiency of 19.8% reported.

### 3.2 Reduced dimensionality perovskites

Layered perovskites have recently become of interest as a route to increased stabilities.<sup>92</sup> As previously discussed, incorporating large organic cations in the synthesis of MAPI results in lower

dimensionality structures, where the cations cannot fit within the perovskite cage.<sup>32,33</sup> In these structures, the large cations are sandwiched between slabs of  $\text{PbI}_6$  octahedra, effectively “capping” the perovskite layers.<sup>93</sup> The resulting two-dimensional (2D) structures, or Ruddlesden–Popper like phases, appear to be stabilised by van der Waals interactions between the capping molecules.<sup>94–97</sup> Similar to MAPI, the physical and structural properties of these compounds can be fine tuned through tailoring of the organic cation, halide and metal components.<sup>31,70</sup> By adjusting the stoichiometric quantities of the bulky organic cation *versus* lead iodide ( $\text{PbI}_2$ ) and methylammonium iodide ( $\text{CH}_3\text{NH}_3\text{I}$ , MAI), the number of layers of perovskite octahedra in each slab ( $n$ ) for the series  $\text{PEA}_2(\text{CH}_3\text{NH}_3)_{n-1}\text{Pb}_n\text{I}_{3n+1}$ , can be controlled.<sup>98</sup> In this way, the limit  $n = \infty$  represents a cubic 3D perovskite,  $n = 1$  corresponds to a 2D layered structure and  $n > 1$  describes “quasi-2D” perovskite structures (Fig. 2e).

A range of intercalated organic–inorganic lead, tin, and germanium perovskites were first structurally characterised in the 1990’s by Mitzi *et al.*, who noted the role of the large cations in aiding thermal and chemical stability, as well as influencing optical and electronic properties.<sup>93–95,98–104</sup> Generally, upon moving from the 3D perovskite structure to the 2D  $n = 1$  phase, the optical band gap widens considerably and n-type conductivity decreases. This is partially a result of the high exciton binding energies (often  $> 300$  eV)<sup>101,105</sup> seen in these structures, which



arise due to spatial restrictions and dielectric mismatch between the organic and inorganic layers.<sup>106,107</sup> In the context of solar cells, this combination of properties is undesirable as it limits  $V_{oc}$  and is likely to result in impaired performance. Stability, on the other hand, is found to be highest for the 2D structures and decrease with increasing values of  $n$ . As such, the primary challenge presented by reduced dimensionality perovskites is to optimise stoichiometry, so as to balance stability against electronic and optical performance.

One route to producing suitable 2D perovskites is through introducing enhanced halogen or hydrogen bonding at the organic–inorganic interface, which results in a red shifting of the band gap due to a more disperse valence band maximum.<sup>108,109</sup> The first layered perovskites put to use in solar cell applications adopted a different approach, instead tuning the band gap through judicious choice of organic cation along with careful stoichiometric control. Smith *et al.* employed bulky  $C_6H_5(CH_2)_2NH_3^+$  (PEA) as the organic cation, producing films with 3 perovskite layers ( $n = 3$ ), an optical band gap of 2.1 eV and reasonably small exciton binding energies (40 meV).<sup>110</sup> Their cells displayed efficiencies up to 4.73% and were stable after 40 days in air with 52% humidity. Similarly, Cao *et al.* produced  $n = 3$  devices containing  $CH_3(CH_2)_3NH_3^+$  via a simple one-step spin-coating process, that exhibited strong light absorption, smooth film surfaces and efficiencies of 4.02%.<sup>111</sup>

The initial attempts at producing 2D perovskite devices suffered from poor charge carrier extraction that limited their efficiencies.<sup>110,111</sup> Recently, Quan *et al.* have demonstrated the first certified hysteresis-free planar perovskite solar cell, containing a 2D absorbing layer.<sup>96</sup> Using a combination of density functional theory (DFT) calculations and complementary studies on physical and optoelectronic properties, the number of perovskite layers was optimised to  $40 < n < 60$ . As expected, van der Waals interactions between the PEA molecules were found to drive increased stability, with the forces acting to reduce the desorption rate of MAI (a key decomposition pathway in MAPI)<sup>112–114</sup> by 6 orders of magnitude. Interestingly, the trend in optical band gap (decreasing with increasing  $n$ )<sup>93</sup> was found to result from a gradual shift in the conduction band minimum, with the valence band maximum effectively fixed in energy. The resulting quasi-2D devices combined the stability of 2D perovskites with the excellent charge-carrier transport and optical properties of MAPI, resulting in a PCE of 15.3% for the composition where  $n = 60$ .<sup>96</sup> Another recent paper has succeeded in producing layered perovskite films orientated such that the sheets form perpendicular with respect to the substrate.<sup>115</sup> This further motivates the development of layered perovskite as it enables clear carrier extraction pathways from the absorber layer to the device contacts.

The last year has seen the substitution of iodine for thiocyanate ( $SCN^-$ ) emerge as an avenue to improving the stability of MAPI whilst retaining high efficiencies.<sup>71,116,117</sup> Inclusion of small amounts of  $SCN^-$ , a pseudo-halide with an ionic radius similar to that of  $I^-$  (217 pm vs. 220 pm),<sup>118</sup> has been shown to produce cells with larger crystal sizes and fewer trap states.<sup>119</sup> Furthermore, the reaction of MAI and  $Pb(SCN)_2$  produces the

compound  $(CH_3NH_3)_2Pb(SCN)_2I_2$  (MAPSI),<sup>120</sup> which is similar in structure to the  $n = 1$  layered perovskites but with  $Pb^{2+}$  octahedrally coordinated to four equatorial  $I^-$  and two axial  $SCN^-$  ions (Fig. 2e).<sup>121</sup> A debate exists as to the size of MAPSI's optical band gap: several studies have reported a direct optical gap of 1.57 eV,<sup>119,121</sup> however a recent paper by Xiao *et al.* demonstrated a thin film possessing direct and indirect optical band gaps of 2.04 eV and 2.11 eV, respectively.<sup>122</sup> Similarly, Umeyama *et al.* also report a larger band gap for MAPSI, noting a red-to-black piezochromic response upon compression (Fig. 2g).<sup>91</sup> The exact cause of this discrepancy has not yet been elucidated, however it has been suggested that contamination of MAPSI with MAPI may play a role. Similar to other 2D perovskites, the layered structure results in an increased enthalpy of formation, bestowing MAPSI with increased chemical stability.<sup>68</sup> Devices containing MAPSI have recorded efficiencies up to 8.3%, with a larger  $V_{oc}$  and enhanced stability in air with 95% humidity than comparable MAPI films.<sup>120</sup> Additionally, it should be possible to tune MAPSI through incorporating other pseudo-halides (such as OCN and SeCN), halides (Cl, Br, I), and metals (Sn, Ge), opening up the possibility for a range of MAPSI structured analogues.<sup>68</sup>

### 3.3 Photoactive organic cations

When the size of the organic cation is increased further still, interconnectivity of the lead iodide octahedral becomes difficult due to large steric effects, and zero-, one-, or two-dimensional (0D, 1D, or 2D) structures result.<sup>104,123</sup> These topologies, characterised by clusters (0D), nanowires (1D), and corrugated sheets (2D) often possess excellent stability but suffer from wide band gaps and poor charge carrier mobilities, due to the lack of clear conduction pathways within the crystal.<sup>124–127</sup> An emerging route to overcoming such properties is the use of photoactive organic cations, primarily those containing aromatic moieties, which can contribute to the optical response of the material.<sup>128,129</sup> Here, shrewd choice of cation is essential to ensure a significant interaction between the organic and inorganic components, and result in broad band spectral absorption.<sup>130,131</sup>

Maughan *et al.* have recently employed the aromatic cycloheptatrienyl ( $[C_7H_7]^+$ , tropylium) ion<sup>128</sup> due to its strong absorption, electronic sensitivity (allowing for optical fine-tuning) and chemical stability, which make it likely to interact favourably with an inorganic system.<sup>132,133</sup> The resulting compound,  $C_7H_7PbI_3$ , forms a nanowire-type structure composed of edge-sharing  $PbI_6$  octahedra, with the tropylium ions distributed between the wires (Fig. 3a). DFT calculations show that the band gap results from charge transfer between the inorganic and organic components, however, its band gap of 2.15 eV is too large for a high efficiency solar absorber. A similar system has been demonstrated using a significantly bulkier organic ligand,  $N,N'$ -di(4-pyridyl)-1,4,5,8-naphthalene diimide (DPNDI), in which nanowires of face-sharing lead iodide octahedra are encased by an interwoven network of protonated DPNDI molecules (Fig. 3b).<sup>134</sup> Beneficial hydrogen bonding and anion– $\pi$  interactions act to reduce the distance between the ligand and





**Fig. 3** (a) Band decomposed charge densities of tropylium tin iodide and tropylium lead iodide, indicating the highest occupied band (HOB) and lowest unoccupied band (LUB) for each material. Reprinted with permission from ref. 128. Copyright 2015, American Chemical Society. (b)  $(\text{Pb}_2\text{I}_6)\cdot(\text{H}_2\text{DPNDI})\cdot(\text{H}_2\text{O})\cdot(\text{NMP})$  viewed along the  $a$  and  $b$  axes, illustrating the 1D lead iodide nanowires and DPNDI network. Reprinted with permission from ref. 135. (c) Quantum-dot-in-perovskite model. Favourable lattice matching between the PbS quantum dot and lead iodide perovskite allows for efficient heteroepitaxial growth in both the  $X$ - $Y$  and  $X$ - $Z$  planes. Reprinted with permission from ref. 138. Copyright 2015, Nature Publishing Group.

nanowire, enabling a material with an ideal band gap of 1.27 eV and unusually long-lived charge-separated states. The efficient charge-carrier separation is expected to lead to reduced recombination losses, however, the loss in dimensionality results in high effective masses and therefore is likely to adversely affect electron mobilities.<sup>135</sup>

Materials comprising mixed inorganic and organic connectivity have been suggested as one method of countering poor mobilities. By designing systems in which charge carriers are mobile in both the inorganic network along with an overlapping network of  $\pi$ -stacked photoactive organic ligands, multiple pathways for carrier extraction can be developed.<sup>136</sup> This has recently been realised in systems containing 1D lead iodide chains coordinated to large aromatic dipyrrodo- and benzodipyrrodo-phenazine compounds, which form eclipsed channels connecting the inorganic chains.<sup>137</sup> It was found that photoexcitation effects charge transfer from the lead iodide component to the organic moiety, however the large band gaps of the materials (2.13 eV and 2.52 eV) prevents their use in photovoltaic applications. While it is clear that this system

highlights the viability of the technique, further optimisation of the organic component to produce the desired optical response and structure directing effects is essential.

### 3.4 Lead(n) chalcogenides

PbS is a quintessential lone pair absorbing material, having been studied for over a decade for use in quantum dot (QD) sensitized solar cells due to its high absorption coefficient, stability in air and ability to generate and split multiple excitons.<sup>139–143</sup> Furthermore, PbS possesses a large Bohr exciton radius of 18 nm, enabling QDs with excellent charge carrier mobilities and a highly tunable band gap.<sup>144,145</sup> The band alignment of PbS QDs can be engineered through the use of different ligand treatments<sup>146,147</sup> and has enabled rapid advancement in PbS solar cells, with a maximum certified efficiency of 9.2%.<sup>148</sup> PbS has also been employed in a core/shell configuration with CdS, which aids surface passivation and has enabled efficiencies up to 5.6% with an enhanced open circuit voltage of 0.66 V.<sup>149</sup>

The highly tunable band gap of PbS (from 0.7 eV to 1.5 eV) means it is possible to produce QDs that absorb in the near- or mid-infrared portion of the solar spectrum, which, when combined with hole conducting polymers that absorb in the UV-visible range, allows for broad spectral coverage.<sup>150</sup> Lu *et al.* produced PbS polymer:nanocrystal composites, based on a donor-acceptor polymer, leading to efficiencies of 4.8% with efficient charge separation from PbS to the polymer and enhanced colloidal stability.<sup>151</sup> PbS has similarly been employed in perovskite solar cells, functioning simultaneously as a co-sensitiser and hole transporting material, enabling cells with a panchromatic response, high photocurrent densities up to 24 mA cm<sup>-2</sup> and efficiencies of 3.6%, despite low open circuit voltages of 0.34 V.<sup>152</sup> By tuning the band alignments of the PbS QDs, a dramatically increased  $V_{\text{OC}}$  of 0.86 V was achieved, resulting in cells with a PCE of 7.5%.<sup>153</sup> Remarkably, due to favourable lattice matching, preformed PbS quantum dots have been incorporated whole into the MAPI structure, producing epitaxially aligned “dots-in-a-matrix” crystals (Fig. 3c).<sup>138</sup> The resulting heterocrystals possessed a modulated optical response, which, when decomposed, indicated that the properties of the QDs and perovskite matrix remained otherwise unaltered. However, the small band gap of the QDs employed (1 eV) and the highly efficient transfer of photo-excited charge carriers from the perovskite to the PbS nanocrystals, while useful for infra-red applications, limits the applicability of the system with regard to solar power generation.

The closely related compounds, PbSe and PbTe, are also of intense interest as a quantum dot solar absorbers, partly due to their even larger Bohr radii of 46 nm<sup>154</sup> and 152 nm,<sup>155</sup> which when coupled with well established and finely size-tunable synthesis methods, enables precise control over the band gap from 0.4–1.4 eV.<sup>156</sup> Pb-based QD solar cells are additionally attractive due to their enhanced stability in air when compared to other solar absorbers. Indeed, the maximum recorded efficiency for a PbSe-based QD solar cell of 6.2% was obtained in devices fabricated in an ambient atmosphere, demonstrating the stability of these devices.<sup>157</sup> Furthermore, previous studies



on PbS have demonstrated its stability in air over 1000 hours of light illumination without device encapsulation.<sup>158</sup> As such, it is clear that lead salts such as PbS and PbSe have an important role to play in the future of colloidal quantum dot photovoltaics. The low cost of raw materials<sup>7</sup> combined with their significant versatility guarantees that Pb-based quantum dot cells will remain a highly studied class of materials.

## 4 Tin absorbers

Lead-based photovoltaics, while generally the highest performing  $ns^2$  solar absorbers, have come under significant scrutiny due to concerns over the toxicity of lead.<sup>159</sup> It is important to note that within the EU, commercial solar cells are exempt from the Restriction of Hazardous Substances Directive and, as such, are not subject to regulation over their lead content.<sup>160</sup> Regardless, the intrinsic instability of MAPI<sup>64</sup> presents the risk that toxic material may be released into the environment unless devices are sufficiently encapsulated, necessitating an increase in the cost of device fabrication.<sup>59,161,162</sup> The last few years have therefore seen a concerted effort to eliminate the use of lead in photovoltaic devices. In this regard, tin is of considerable interest as it is both cheap and non-toxic,<sup>163</sup> and, being a group 14 metal, is expected to show much of the same coordination chemistry and electronic properties seen in the lead analogues. Consequently, materials containing tin have long been sought after as a route to an earth-abundant and non-toxic solar absorber.

### 4.1 Perovskite structured

Due to the successes of the lead hybrid perovskites there has been a significant research effort towards synthesising and evaluating the tin analogues. Unfortunately, the propensity for  $\text{Sn}^{2+}$  to undergo oxidation to  $\text{Sn}^{4+}$  has proved challenging to overcome and still represents a major decomposition mechanism in the tin hybrid perovskites.<sup>39,167</sup> Initially, partial substitution of Pb with Sn to form  $\text{CH}_3\text{NH}_3\text{Sn}_{0.25}\text{Pb}_{0.75}\text{I}_3$  enabled a reduction in band gap relative to MAPI, with devices showing efficiencies up to 7.37%.<sup>168,169</sup> In an attempt to counteract the low photocurrent densities resulting from poor film coverage,  $\text{PbCl}_2$  was added to produce planar  $\text{CH}_3\text{NH}_3\text{Sn}_n\text{Pb}_{1-n}\text{I}_{3-x}\text{Cl}_x$  based cells with 10.1% efficiency.<sup>170</sup> In 2016, mixed Pb–Sn perovskite films with the composition  $\text{CH}_3\text{NH}_3\text{Sn}_{0.5}\text{Pb}_{0.5}\text{I}_3$  achieved efficiencies of 13.6%, demonstrating the potential of devices with reduced lead content to achieve high performance.<sup>171</sup>

It was originally thought that the presence of Pb was essential to prevent undesirable oxidation of Sn, however, in 2014, two groups were successful in yielding solar cells based on the completely lead-free  $\text{CH}_3\text{NH}_3\text{SnI}_3$ .<sup>172,173</sup> These devices, with efficiencies of 5.23%<sup>172</sup> and 6.4%,<sup>173</sup> were made possible through rigorous glovebox protocols and ultra-high purity starting materials.  $\text{CH}_3\text{NH}_3\text{SnI}_3$  possesses an optical band gap of 1.30 eV<sup>39,74</sup> and, similarly to MAPI, is intrinsically p-type, with relatively high carrier densities ( $10^{19} \text{ cm}^{-3}$ ).<sup>174</sup> Devices based on a  $\text{CH}_3\text{NH}_3\text{SnI}_3/\text{SiO}_2$  nanocomposite architecture have shown impressive open circuit voltages up to 0.88 V, only

350 mV less than the thermodynamic limit.<sup>173</sup> However, small carrier diffusion lengths (30 nm) along with poor long-term stability present a significant obstacle to overcome before these devices can find practical applications.<sup>90</sup>

In 2015, Koh *et al.* revealed that inclusion of  $\text{SnF}_2$  in the synthesis of formamidinium tin iodide ( $\text{HC}(\text{NH}_2)_2\text{SnI}_3$ , FASI) counteracts the facile oxidation of tin by promoting the reduction of  $\text{Sn}^{4+}$  to  $\text{Sn}^{2+}$ , however, this increased resilience to oxidation occurs at the cost of decreased conductivity.<sup>175</sup> This technique enabled, for the first time, the production of FASI-based solar cells with power conversion efficiencies up to 2.1%. FASI has an ideal band gap of 1.4 eV and, unlike the analogous lead compound, FAPI, does not possess any other thermally accessible phases that can cannibalise device performance.<sup>74,77,176</sup> Indeed, the stability of FASI has been demonstrated up to 200 °C, well above maximum device operating temperatures.<sup>175</sup> Recently, this technique has been extended to prevent phase segregation on the surface of the films through the formation of a  $\text{SnF}_2$ –pyrazine complex, yielding devices with power conversion efficiencies of 4.8% (Fig. 4a).<sup>164</sup> These films displayed smoother surface morphologies and exhibited longer recombination lifetimes than reference cells prepared in the absence of pyrazine. Impressively, encapsulated devices stored in ambient conditions showed stable performance for over 100 days, with a loss in efficiency of only 2% over this period. Currently, however, a combination of low open circuit voltage (0.32 V) and fill factor (63%) prevent these devices from achieving performance comparable with other perovskite technologies.<sup>164</sup>

The issue of unwanted oxidation has also plagued the all-inorganic perovskite,  $\text{CsSnI}_3$ . First used as a solid-state hole transporting material in dye-sensitised solar cells,<sup>177</sup>  $\text{CsSnI}_3$  is a p-type semiconductor with a band gap of 1.30 eV.<sup>178,179</sup> The first planar heterojunction devices employing  $\text{CsSnI}_3$  as the absorber material demonstrated power conversion efficiencies up to 0.9%, but were inhibited by poor stability and the polycrystalline nature of the films.<sup>180</sup> Subsequent studies have, similarly to the other tin perovskites, employed  $\text{SnF}_2$  as an additive to control the oxidation state of tin, enabling efficiencies of 2.0% and high photocurrents of  $22.7 \text{ mA cm}^{-2}$ .<sup>165,181</sup> In these cells, performance was severely restricted by low open circuit voltages of 0.24 V, about 4 times less than those seen in typical MAPI devices.<sup>182,183</sup> This has been partially mediated through the substitution of iodine with bromine to form  $\text{CsSnI}_{3-x}\text{Br}_x$ , enabling higher open circuit voltages due to blue shifting of the band gap (Fig. 4b).<sup>165</sup> Unfortunately, unlike in the lead hybrid perovskites where inclusion of bromine has been shown to increase stability in humid conditions,<sup>85,184</sup> no such resistance is conferred in the case of  $\text{CsSnI}_3$ , with the oxidation of  $\text{Sn}^{2+}$  to  $\text{Sn}^{4+}$  remaining the primary chemical instability. Additionally, alongside problems relating to unwanted oxidation,  $\text{CsSnI}_3$  also possesses an alternative 1D yellow phase, with a band gap of 2.6 eV, formed under exposure to air or organic solvents.<sup>178,185,186</sup> As such, it is clear that significant work is needed to improve the stability of  $\text{CsSnI}_3$  based devices if they are to find practical applications.





Fig. 4 (a) *J*-*V* curves and trend in band gap demonstrating the effect of pyrazine and concentration of SnF<sub>2</sub> of FASn<sub>3</sub> perovskite solar cells. Adapted with permission from ref. 164. Copyright 2016, American Chemical Society. (b) Trend in band gap and *J*-*V* curves for CsSn<sub>1-x</sub>Br<sub>x</sub> perovskite solar cells, where *x* = 0 to 3. Adapted with permission from ref. 165. Copyright 2015, American Chemical Society. (c) Crystal structures of tin monosulfide. The lowest energy structure is herzenbergite (*Pnma*), a distorted rocksalt structure (*Fm* $\bar{3}$ *m*). Several reports have identified tin monosulfide in the zincblende crystal structure (*F* $\bar{4}$ *3m*), however, DFT calculations reveal this phase to be high in energy. Adapted with permission from ref. 166. Copyright 2012, American Chemical Society.

## 4.2 Tin(II) chalcogenides

Tin(II) monosulfide (SnS) possesses many of the ideal properties for a highly efficient solar absorber, such as a high absorption coefficient greater than  $10^4 \text{ cm}^{-1}$  and carrier concentrations around  $10^{17}$ – $10^{18} \text{ cm}^{-3}$ .<sup>187–191</sup> However, despite these properties and over 20 years of active research,<sup>192</sup> the efficiency of SnS-based devices has yet to reach 5%.<sup>193,194</sup> Nonetheless, the abundance of tin and sulphur, combined with the ease of materials processing and a maximum predicted efficiency of 32% (as per the Shockley–Queisser limit),<sup>195</sup> make SnS attractive as a candidate photovoltaic absorber. SnS possesses an indirect fundamental band gap of 1.1 eV,<sup>196–198</sup> however, its optical absorption (onset at  $\sim 1.3$  eV) remains high due to its slightly larger direct band gap of 1.2–1.5 eV, suggesting that the indirect gap is not detrimental to performance.<sup>192,199–201</sup> SnS is intrinsically p-type, with low hole effective masses ( $m_{\text{h}}^* = 0.2 m_0$  in the *a* and *b* directions;  $m_{\text{h}}^* = m_0$  along *c*) and is generally employed in a p–n junction architecture using ZnO or CdO as the n-type layer.<sup>190</sup> Unlike PbS, the small Bohr radius of SnS (7 nm) precludes its use in quantum dot solar cells.<sup>202</sup>

Several distinct phases of tin(II) monosulfide are known,<sup>188,203–205</sup> with the most stable room temperature structure being herzenbergite, a distorted rock salt structure ( $\alpha$ -SnS, *Pnma*).<sup>166</sup> The distortion of the lattice from a cubic to orthorhombic structure is due to the strong Sn 5s<sup>2</sup> lone pair (following the revised lone pair model)<sup>206,207</sup> which repel and result in the formation of a layered system held together by weak covalent interactions (Fig. 4c). This 2D structure is the source of the anisotropy seen in the hole effective masses.<sup>190</sup> Thin films of SnS have been produced by a wide range of deposition techniques,

including chemical bath deposition (CBD),<sup>208–210</sup> atomic layer deposition (ALD),<sup>211,212</sup> spray pyrolysis,<sup>213–215</sup> and thermal evaporation,<sup>216,217</sup> of which the latter two techniques are most common. Choice of deposition method can have a profound impact on the optoelectronic properties of the films, with CBD, ALD and vapor transport deposition generally producing films with the largest carrier concentrations and highly mobile holes.<sup>188,218</sup> It should be noted that the variation in microstructure is large, even within the same deposition method, and is expected to be a primary factor in determining the efficiency of the films, due to the predominant formation of small structures with large grain boundaries between crystallites.<sup>219–222</sup>

Sinsersuksakul *et al.* have reported the most efficient SnS-based solar cell to date, producing a cell with a PCE of 4.4%.<sup>193</sup> Their device, along with the other highest performing SnS solar cells, employed Mo as the metallic contact and ZnO as the n-type transparent electrode, with the addition of an optimised Zn(O,S) buffer layer necessary to achieve high performance.<sup>223,224</sup> Interestingly, Burton *et al.* have shown Mo to be unsuited as a back contact material due to the small ionisation potential of SnS (4.7 eV), instead suggesting metals with lower workfunctions, such as Ti, W, or Sn, as optimal contact materials.<sup>225</sup> Other reports, based on impedance spectroscopy measurements, indicate Mo performs poorly due to increased series resistance and high rates of tunnelling assisted recombination and have recommended Cu as a viable alternative.<sup>226</sup>

There has been some controversy surrounding the reports of zincblende structured SnS (*F* $\bar{4}$ *3m*) deposited as microparticles and thin-films (Fig. 4c).<sup>188,194,203,227</sup> Such a material would allow for extended compatibility with existing II–VI and III–V





However, this precludes direct integration into the AMX<sub>3</sub> formula—instead, we review the wide variety of antimony compounds that have been studied for photovoltaics.

### 6.1 Antimony chalcogenides

The binary antimony chalcogenides have seen a great deal of research interest over the past 35 years, yet despite this interest, cell efficiencies remain below 10%. Both Sb<sub>2</sub>S<sub>3</sub> and Sb<sub>2</sub>Se<sub>3</sub> share a crystal structure consisting of 1D nanowires formed from Sb<sub>4</sub>Ch<sub>6</sub> units, with the nanowires bound by weak Ch–Ch interactions. The Sb s<sup>2</sup> lone pair is stereochemically active, forming a square pyramidal coordination around Sb, with the lone pair occupying space in-between the nanowires.<sup>254,255</sup> This low dimensionality may be expected to reduce the overall functionality as an absorber material, however despite this, Sb<sub>2</sub>S<sub>3</sub> and Sb<sub>2</sub>Se<sub>3</sub> have both seen significant interest from the PV community.

Perhaps due to its simplicity, antimony sulfide has had a long, storied history as a photovoltaic absorber: thin films of Sb<sub>2</sub>S<sub>3</sub> were examined photoelectrochemically in 1982 with PV applications in mind,<sup>256</sup> however cells remained sparse until Savadogo and Mandal produced a series of n-Sb<sub>2</sub>S<sub>3</sub> cells in the 1990's, ranging from a 3.9% efficient photoelectrochemical cell to 7.3% in a heterojunction with p-Ge and deposited with silicotungstic acid.<sup>257–259</sup> Despite these prior successes, Sb<sub>2</sub>S<sub>3</sub> only recently experienced a resurgence upon its use as a sensitizer with TiO<sub>2</sub> and p-CuSCN as the hole transporting material (HTM), attaining efficiencies near 5%.<sup>260–263</sup> Since, Sb<sub>2</sub>S<sub>3</sub>-sensitized cells have seen much work, as Seok and others have made recent strides in bringing efficiencies up to 7.5%<sup>264–267</sup> in inorganic–organic heterojunction cells. This has largely been through the reduction of trap sites, however, there still remains a large V<sub>oc</sub> deficit limiting the growth of these cells. Measurements at low light have seen higher efficiencies of 8–9%, however the lack of comparable measurements with other materials makes this difficult to compare.<sup>268</sup> With a high near-direct band gap of near 1.7 eV, and a high absorption coefficient,<sup>269,270</sup> and multiple deposition techniques available,<sup>271,272</sup> Sb<sub>2</sub>S<sub>3</sub> remains a promising candidate material. First principles calculations have replicated the experimental band gap well, using hybrid DFT and meta-GGA functionals,<sup>273,274</sup> and have identified that the valence electrons remained confined to the individual chains, but are diffuse within them: this dispersion indicates that the charge carriers should remain mobile.<sup>275,276</sup>

Despite the relative success of Sb<sub>2</sub>S<sub>3</sub>, within the last few years, there have been movements to develop the isostructural antimony selenide instead. Sb<sub>2</sub>Se<sub>3</sub> has a lower band gap, around 1.1–1.3 eV in both nanostructures<sup>277</sup> and thin films,<sup>278–280</sup> than Sb<sub>2</sub>S<sub>3</sub> and retains a high optical absorption coefficient of ~10<sup>5</sup> cm<sup>-1</sup>.<sup>279–281</sup> This high absorption may disguise a fundamental indirect band gap, which is only slightly lower in energy, as observed *via* DFT,<sup>282</sup> quasiparticle band structure calculations,<sup>276</sup> and UV-vis<sup>283</sup> and so, like the sulfide, Sb<sub>2</sub>Se<sub>3</sub> has been referred to as a 'effectively direct band gap' semiconductor. Additionally, theoretical band alignment with TiO<sub>2</sub> indicates that with improvements in V<sub>oc</sub>, the lower band gap (and thus high possible J<sub>sc</sub>) of Sb<sub>2</sub>Se<sub>3</sub> compared to

Sb<sub>2</sub>S<sub>3</sub> could lead to higher attainable efficiencies in pnictogen-chalcogenide sensitised solar cells.<sup>284</sup>

Other than a <1% efficiency cell in 2002,<sup>278</sup> almost all advances in Sb<sub>2</sub>Se<sub>3</sub> cells began in 2014, with the publication of a TiO<sub>2</sub>-sensitized inorganic–organic cell of 3.2% from Choi *et al.*<sup>285</sup> and a 1.9% thin film CdS/Sb<sub>2</sub>Se<sub>3</sub> cell.<sup>286</sup> Since then, Tang and co-workers have driven the development of the thin film architecture, reaching 3.7% by the end of 2014,<sup>287,288</sup> and 5.6% in 2015.<sup>243,289</sup> Additionally, they have indicated that vertically aligned growth of the 1D structure of Sb<sub>2</sub>Se<sub>3</sub> means that high carrier transport can be maintained throughout the Sb<sub>2</sub>Se<sub>3</sub> layer, while grain boundaries in the material will form parallel to the chains, making them inherently benign, reducing a major source of losses in polycrystalline cells (Fig. 6a).<sup>243</sup> This applies to many other antimony and bismuth(III) materials, including Sb<sub>2</sub>S<sub>3</sub> but also SbSI and the other members of the V–VI–VII series, where the stereochemically active lone pair enforces a 1-D topology—this presents a major advantage for the future development of these materials in photovoltaics.

In addition to the binary sulfides, a smaller section of work has examined the solid solution between the sulfide and selenide—with a tunable band gap between 1.3–1.7 eV,<sup>290</sup> and high absorption in both binary systems, this presents an opportunity for tunable photovoltaic materials. Despite low initial efficiencies below 1%,<sup>291</sup> recent work has used the advances in deposition techniques and the adoption of poly(3-hexylthiophene) (P3HT) as an efficient hole transporting material to attain an efficiency of 6.6%, close to the most successful Sb<sub>2</sub>S<sub>3</sub> cells.<sup>292</sup>

### 6.2 Antimony chalcogenides

The ternary antimony chalcogenides adopt a 1D structure very similar to that of the simple chalcogenides mentioned above: the antimony atoms occupy a pseudo-square pyramidal configuration with sulfur and iodine in a dimeric unit that infinitely repeats along *a*, with the stereochemically active lone pair occupying the final position in the Sb octahedron.<sup>293</sup> What distinguishes SbSI from the binary chalcogenides, however, is its photoferroicity: SbSI undergoes a ferroelectric phase transition,<sup>294</sup> giving a phase with spontaneous polarization, allowing for anomalous photovoltaic effects beyond that of usual semiconductors, with the potential for very high V<sub>oc</sub>. Walsh and co-workers discuss this in their 2015 work,<sup>54</sup> also calculating its electronic structure—like Sb<sub>2</sub>S<sub>3</sub>, it possesses a slightly indirect band gap of around 1.9 eV, in concordance with experiment,<sup>295</sup> but also low effective masses. Despite this, as the authors highlight, SbSI and SbSeI have so far been passed over for other materials. In 2016, Walsh and co-workers revisited the V–VI–VII compounds, including SbSBr, using quasiparticle GW theory, obtaining mostly similar band gaps in addition to band alignments—this should allow for semiconductor contacts to be tailored for these materials.<sup>296</sup>

### 6.3 Copper antimony chalcogenides

In contrast, the ternary copper antimony chalcogenides have seen a great deal of interest in photovoltaic applications.



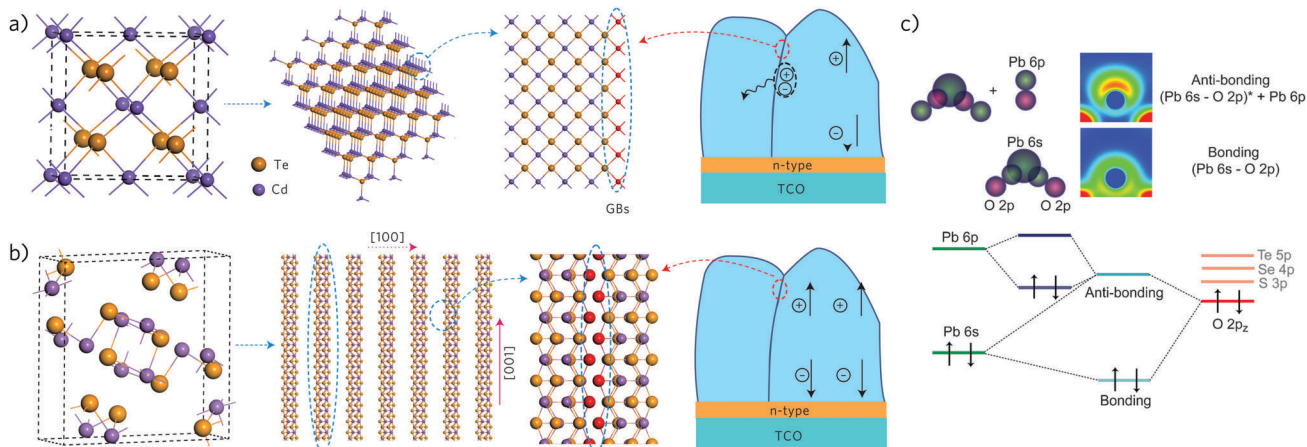


**Fig. 6** (a and b) The role of grain boundaries (GBs) as recombination centres in CdTe and  $\text{Sb}_2\text{Se}_3$  solar cells. (a) The 3D structure of CdTe results in dangling bonds at GBs (illustrated by red rods), which act as defects that can cause unwanted recombination of charge carriers. (b) In contrast, the 1D ribbon structure of  $\text{Sb}_2\text{Se}_3$ , if oriented in the [001] direction, permits benign GBs due to saturation of the terminal atoms (red spheres). (a and b) Reprinted with permission from ref. 243. Copyright 2015, Nature Publishing Group. (c) Schematic of the orbital interactions that result in the formation of the stereochemical lone pair in PbO (top panel) and the corresponding molecular orbital diagram (bottom panel). Reprinted with permission from ref. 207.

$\text{CuSbS}_2$  has seen perhaps the most attention—Nair and co-workers investigated p-type  $\text{CuSbS}_2$  in combination with intrinsic  $\text{Sb}_2\text{S}_3$  to create a p-i-n device in 2005,<sup>297</sup> however the early stage of development meant both the  $J_{\text{sc}}$  and  $V_{\text{oc}}$  were relatively low. Fundamentally, however,  $\text{CuSbS}_2$  displays suitable electronic properties, with a band gap measured around 1.5 eV<sup>298</sup> and good carrier mobilities of 20 to 49  $\text{cm}^2 \text{V}^{-1} \text{s}^{-1}$ , although high conductivity has been found to be strongly dependent on the precise composition.<sup>253,299</sup> Additionally, synthesis has been possible via a number of deposition and chemical routes.<sup>300–302</sup> Its crystal structure, together with  $\text{CuSbSe}_2$ , is related to the 3D chalcopyrite structure of the successful photoabsorber  $\text{CuInSe}_2$ , however the greater stereochemical effect of the Sb  $s^2$  lone pair causes a distortion, resulting in a layered structure (Fig. 7a).<sup>303</sup> Walsh *et al.*, using DFT calculations, have discussed the electronic and structural effect of the lone pair in these materials: in concordance with the revised lone pair effect model for post-transition metal compounds,<sup>207</sup> the antimony s states mix with the sulfur p states to allow further mixing with antimony p states, leading to antibonding states close to the top of the

valence band and the structural distortion (Fig. 6b). This study also finds the band gaps to be indirect, although like the binary chalcogenides, only by 0.1–0.2 eV. This has been supported by subsequent theoretical work,<sup>304,305</sup> which have additionally evaluated high absorption coefficients ( $> 10^5 \text{ cm}^{-1}$ ). Yu *et al.* corroborated these results, and used them to indicate that  $\text{CuSbS}_2$  and  $\text{CuSbSe}_2$ , by possessing relatively flat band edges with a high Density of States there, will give stronger absorption than the well-known absorber  $\text{CuInSe}_2$ .<sup>57</sup> Using their metric of spectroscopically limited maximum efficiency (SLME), which improves upon the Shockley–Queisser limit by including non-radiative effects and film absorption, the SLMEs of  $\text{CuSbS}_2$  and  $\text{CuSbSe}_2$  were 23% and 27% respectively, comparable to or higher than that of  $\text{CuInSe}_2$ . Cell efficiencies have, so far, have been unable to reach this level:  $\text{CuSbS}_2$  has improved significantly from that initial cell with multiple cells, either with CdS or sensitizing  $\text{TiO}_2$ , now exceeding 3%,<sup>306–308</sup> and  $\text{CuSbSe}_2$  has matched this, with cells of 1.3% and 3.5%<sup>309,310</sup> published so far. However, recently two strategies have seen improvements in  $\text{CuSbS}_2$  cells: annealing in  $\text{Sb}_2\text{S}_3$  vapour followed by KOH etching was seen to almost double  $J_{\text{sc}}$ ,  $V_{\text{oc}}$  and fill factors, while using a co-evaporation fabrication method lead to the highest recorded open-circuit voltage of 526 mV.<sup>311,312</sup> With the suitable optical and electronic properties seen above, and Yang *et al.* finding few deep defect levels to act as recombination centres,<sup>253</sup> further growth in this area may well be possible (Fig. 7b).



**Fig. 7** (a) Crystal structure and (b) intrinsic defect formation energies of  $\text{CuSbS}_2$ . Adapted with permission from ref. 253. Copyright 2014, American Chemical Society.

#### 6.4 Cesium and hybrid antimony compounds

Perhaps the most relevant antimony compounds to the hybrid perovskite family, however, are the cesium antimony halides and the cesium/methylammonium antimony sulfides. The 2D  $P\bar{3}m1$  phase of  $\text{Cs}_3\text{Sb}_2\text{I}_9$  was recently the subject of study by Saparov *et al.*;<sup>313</sup> it occupies a “defect perovskite” structure, where  $\frac{1}{3}$  of the antimony sites of a hypothetical ‘ $\text{Cs}_3\text{Sb}_3\text{I}_9$ ’



perovskite unit are vacant, creating layers of corner-sharing Sb-I octahedra with a small inter-layer separation. This structure was found theoretically and experimentally to have an indirect 2.05 eV band gap, with carrier effective masses close to  $0.5m_0$  and a high absorption coefficient. However, their prepared thin film cells displayed a  $V_{oc}$  of  $\sim 0.3$  eV and low efficiencies, theorised to be a result of multiple deep defect levels effecting facile non-radiative recombination. Study of the methylammonium hybrid antimony iodide,  $(\text{CH}_3\text{NH}_3)_3\text{Sb}_2\text{I}_9$ , has been primarily limited to spectroscopic studies on the dynamics of the methylammonium cation,<sup>314,315</sup> however 2016 has seen the first production of a cell by Hebig *et al.*, demonstrating an efficiency of 0.5%, improving upon that of the cesium compound.<sup>316</sup> The cell demonstrated a much higher  $V_{oc}$  of 0.90 eV, however a low  $J_{sc}$  of  $1.0 \text{ mA cm}^{-2}$  plus an Urbach tail energy of 62 meV indicating significant disorder in the amorphous absorber layer, suggests optimization of synthesis and cell construction will be required to produce viable cells.

Beyond this, work on hybrid antimony iodides remains limited: while some lower dimensionality perovskites have been reported, electronic characterisation is scarce.<sup>317,318</sup> The antimony sulfides  $\text{Cs}_3\text{Sb}_8\text{S}_{13}$  and  $(\text{MA})_2\text{Sb}_8\text{S}_{13}$  have also come to attention recently in the work of Yang *et al.*,<sup>273</sup> who examined these two compounds with hybrid DFT. Both compounds demonstrate significant similarities with the parent  $\text{Sb}_2\text{S}_3$  phase, such as the stereochemically active lone pair, similar, if higher band gaps, and a multi-valley band structure—which should lead to low radiative recombination, while retaining a high optical absorption.

## 7 Bismuth absorbers

Bismuth is particularly notable as a heavy metal as, unlike its neighbours of lead, polonium and thallium, it demonstrates

very little evidence of toxicity.<sup>319,320</sup> As such, it has seen increasing use in catalysis and organic synthesis as ‘green chemistry’ becomes ever more crucial,<sup>321,322</sup> the rise of the lead halide perovskites in the perovskite community has led to some considering whether bismuth compounds can reach a similar level of success.<sup>129</sup>

### 7.1 Bismuth sulfide

Bismuth sulfide, like the binary antimony chalcogenides, has had a long research history within the solar community, with the first thin films and photoelectrochemical cells being developed in the 1980's.<sup>323,324</sup> Most research on bismuth selenide has focused on its rhombohedral topological insulator phase,<sup>325</sup> as the 1.25 eV orthorhombic phase has only recently been isolated in a single-phase.<sup>326</sup> The use of chemical deposition techniques to produce bismuth sulfide has seen considerable interest since,<sup>327–329</sup> as offering a low temperature, facile synthesis is highly desirable for device manufacture, although the quality and crystallinity of films may suffer compared to evaporation techniques.<sup>330,331</sup> Nevertheless, chemically deposited thin films of  $\text{Bi}_2\text{S}_3$  have been used in combination with lead chalcogenides to produce cells of 0.5% efficiency in 2011,<sup>332</sup> and 2.5% in 2013.<sup>333</sup> With an optical band gap measured between 1.3–1.6 eV experimentally<sup>332,334</sup> and through GW calculations,<sup>276</sup> a high absorption coefficient, and low toxicity elements,  $\text{Bi}_2\text{S}_3$  is a promising material for PV (Fig. 8a).  $\text{Bi}_2\text{S}_3$  is intrinsically n-type,<sup>335</sup> and hence has been particularly successful in heterojunctions with traditional p-type materials, such as crystalline silicon,<sup>336</sup> or PbS quantum dots; the latter devices have neared 5% efficiency with the ‘bulk-nano’ heterojunction architecture leading to much longer carrier lifetimes and quadrupled  $J_{sc}$  in comparison with a bilayer architecture.<sup>337,338</sup> Recently, two areas which have seen particular success are its



**Fig. 8** Crystal structure and band structure of bismuth based solar absorbers: (a)  $\text{Bi}_2\text{S}_3$ —adapted with permission from ref. 335. Copyright 2016, American Chemical Society; and ref. 276. Copyright 2013, American Physical Society (b)  $\text{BiI}_3$ —adapted with permission from ref. 349. Copyright 2015, American Chemical Society; and ref. 350. Copyright 2015, AIP Publishing LLC. (c)  $\text{BiSI}$ —adapted with permission from ref. 351. (d)  $\text{Rb}_3\text{Bi}_2\text{I}_9$  and  $\text{Cs}_3\text{Bi}_2\text{I}_9$ —adapted with permission from ref. 349. Copyright 2015, American Chemical Society.



use as a TiO<sub>2</sub> sensitizer, reaching 2.5% efficiency in 2015,<sup>339,340</sup> and in nanostructures.<sup>341–343</sup> In particular, hybrid solar cells containing nanocrystalline Bi<sub>2</sub>S<sub>3</sub> in combination with the organic absorber P3HT have seen great progress from the group of Konstantatos and others, with cell efficiencies rising from below 1% in 2011 to 3.3% in 2015,<sup>344–346</sup> and the exploration of size-dependent tunability and passivation of surface defects.<sup>347,348</sup>

## 7.2 Bismuth iodide

Like the antimony and bismuth chalcogenides and chalcogenides, bismuth iodide, BiI<sub>3</sub>, was recently highlighted by Brandt *et al.* as a potential solar absorber material due to its suitable band gap and the likelihood of good defect tolerance.<sup>37</sup> Prior to this, its involvement in photovoltaics has been limited—most research has focused on its use as a radiation detector,<sup>352,353</sup> with a single report of its use as a hole-transport layer in organic solar cells, where its performance was observed to be comparable to PEDOT:PSS.<sup>354</sup> Occupying a layered rhombohedral crystal structure,<sup>355</sup> its band gap was the subject of considerable variance, with values ranging from 1.99 eV with ellipsometry to 1.43 eV with DFT calculations (Fig. 8b).<sup>356,357</sup> Podraza *et al.* were able to rationalise this through the low optical absorption obscuring the actual indirect band gap of 1.67 eV, in close agreement with other calculations.<sup>358,359</sup> With a suitable band gap for PV applications, it has thus been the subject of study by Seshadri and co-workers, producing a cell with 0.3% efficiency; the  $V_{oc}$  of this cell was noted to be low due to the poor alignment of BiI<sub>3</sub> with the hole and electron transporting layers.<sup>349,350</sup> Brandt *et al.* have also further studied this compound, finding a much higher absorption coefficient than previously recorded, however photoluminescence revealed an estimated, short carrier lifetime of 180–240 ps which, in combination with a high resistivity of  $\sim 10^8 \Omega \text{ cm}^{-1}$ , is likely to severely hinder conductivity.<sup>360</sup> Recent computational study of BiI<sub>3</sub> monolayers, however, predicted them to be stable, and show significantly improved IR-absorbance in a bilayer with graphene, raising the possibility of photoactive heterostructures.<sup>361</sup>

## 7.3 Bismuth chalcogenides

With analogous 1D crystal structures to their antimony counterparts,<sup>362–364</sup> together with suitable, slightly indirect band gaps of 1.59 eV and 1.29 eV respectively,<sup>365</sup> it is understandable that BiSI and BiSeI should also be considered for photovoltaic applications (Fig. 8c). However, despite interest in its photoconduction and photovoltaic behaviour in the 1960's,<sup>366,367</sup> it is only very recently that the bismuth chalcogenides have been thoroughly assessed in this manner. In 2012, Mullins and co-workers published two studies on this topic—the first of these was a thorough characterization study of BiSI thin films, finding a high absorption coefficient ( $5 \times 10^4 \text{ cm}^{-1}$ ), photocurrents of up to  $5 \text{ mA cm}^{-2}$  under AM1.5G illumination and a maximum  $V_{oc}$  of 370 mV with a  $I^-/I_3^-$  couple.<sup>368</sup> The second examined the effect of selenium doping, allowing for a decrease in band gap of 0.15 eV, and attempted both photoelectrochemical and solid-state cells, with 0.25% and 0.01% efficiency respectively,<sup>369</sup> however BiSI was observed to degrade under

electrochemical conditions. Recent theoretical work has explained the poor solid-state behaviour: the conduction band alignment of BiSI means that the choice of p-CuSCN as the hole transporting material limits  $V_{oc}$  considerably, and there will be poor electron transfer to the FTO electrode, as used by Mullins and co-workers.<sup>351</sup> As such, there should be great potential for improvement—with antibonding states at the valence band maximum, and a high static dielectric constant recently evaluated,<sup>370</sup> BiSI films should possess the high degree of defect tolerance identified by Brandt *et al.* as a highly desirable PV property.<sup>37</sup>

While the bismuth oxyhalide family (BiOX, X = Cl, Br, I) have been investigated for a variety of applications, most notably as photocatalysts for organic pollutant decomposition or water splitting,<sup>371–374</sup> a small number of reports have examined BiOI for photovoltaic applications. BiOI has the lowest band gap of the family, measured between 1.6 eV and 2.0 eV,<sup>372,375,376</sup> meaning that while it demonstrates the weakest photoelectrochemical behaviour,<sup>377</sup> it is also likely the best candidate for photovoltaics. The first attempt at a cell in 2009, using an iodide couple in ethylene glycol attained a moderate  $V_{oc}$  of 461 mV, but a very low short circuit current ( $20.4 \mu\text{A cm}^{-2}$ ), likely due to the poor conduction between the BiOI and its chitosan matrix.<sup>378</sup> Directly coating the FTO electrode with BiOI was observed to increase  $J_{sc}$  by a factor of 10,<sup>379</sup> yet the most significant improvement was seen recently with a similar cell architecture, with a  $J_{sc}$  of  $3.8 \text{ mA cm}^{-2}$  and an efficiency of 1.03%.<sup>380</sup> Interestingly, BiOI has also seen use recently in combination with Bi<sub>2</sub>S<sub>3</sub> as the absorber layer—while short-circuit currents were again above  $1 \text{ mA cm}^{-2}$ , low fill factors meant efficiencies were low.<sup>381</sup> Attempts to utilise BiOCl and BiOBr in other DSSCs have also met with low currents and efficiencies.<sup>382</sup>

## 7.4 Noble metal bismuth chalcogenides and halides

CuBi<sub>2</sub>, like the copper antimony chalcogenides, has seen substantial theoretical interest within the last four years,<sup>40,304,383–386</sup> with much attention paid to the structural effect of the bismuth lone pair, and the high absorption coefficient ( $\sim 10^5 \text{ cm}^{-1}$ )—the band gaps obtained (1.5–1.6 eV) also correlate well with experimental measurements (1.6–1.8 eV).<sup>387,388</sup> Additionally, CuBi<sub>2</sub> has been shown to demonstrate moderate hole mobilities of  $> 10 \text{ cm}^2 \text{ V}^{-1} \text{ s}^{-1}$ ,<sup>389,390</sup> and although previously assigned as an n-type conductor,<sup>387,388</sup> recent theoretical and experimental work strongly suggests it is p-type.<sup>385,390</sup> Despite this substantial effort towards characterisation, however, detailed study of defects and production of a cell remains an open challenge.

Alternate copper bismuth sulfides, on the other hand, have seen a little more success. Interest in Cu<sub>3</sub>BiS<sub>3</sub> from the photovoltaic community mostly began in the 2000's: Estrella *et al.* characterised thin films of Cu<sub>3</sub>BiS<sub>3</sub> in 2003, finding a band gap within 1–1.6 eV, a high optical absorption coefficient ( $> 10^5 \text{ cm}^{-1}$ ) and a photocurrent response;<sup>391</sup> Gerein and Haber were able to replicate the band gap (1.3 eV) and absorption coefficient, in addition to finding low resistivity in high quality annealed films.<sup>392</sup> Since then, experimental studies have examined its photovoltaic behaviour, finding that surface trap states may



be passivated in a heterojunction with  $\text{In}_2\text{Se}_3$ ,<sup>393,394</sup> and its excitonic behaviour through Raman and Photoluminescence measurements.<sup>395</sup> Theoretical results have evaluated the fundamental indirect band gap at around 1.7 eV, but have also reproduced the high absorption coefficient in addition to predicting a relatively low hole effective mass ( $<0.5m_0$ ) and the efficiency improvement on O-doping.<sup>396–398</sup> Most recently, a photoelectrochemical energy conversion efficiency of 1.28% was obtained in a  $\text{Cu}_3\text{BiS}_3$ -sensitized  $\text{TiO}_2$  cell, giving a strong indication of the potential of these materials.<sup>399</sup>  $\text{Cu}_4\text{Bi}_4\text{S}_9$  has also seen particular success as a sensitizer to  $\text{In}_2\text{Se}_3$ , obtaining cells with efficiencies between 3.9% and 6.2% with a variety of oxide contacts, with the  $\text{Cu}_4\text{Bi}_4\text{S}_9$  addition noted to particularly improve the surface photovoltages.<sup>400</sup>

Most notably, however,  $\text{AgBiS}_2$  has seen a massive stride in photovoltaic efficiency very recently, much more so than its copper analogues. Also unlike  $\text{CuBiS}_2$ , nanocrystalline- and high temperature bulk- $\text{AgBiS}_2$  occupies a 3D cubic disordered rocksalt structure,<sup>401,402</sup> which has seen previous interest due to its high temperature order–disorder transition and its effect on thermoelectric behaviour.<sup>403,404</sup> While the bulk has been recorded to have an optical band gap of 0.9 eV,<sup>405</sup> strong quantum confinement effects have meant that quantum dot thin-films have band gaps reported at 1.0–1.3 eV, although with one study reporting 2.67 eV; that study also reports a very strong absorption coefficient above  $10^5$  for low frequencies.<sup>405–407</sup> Despite this, initial  $\text{AgBiS}_2$  QD-sensitized  $\text{TiO}_2$  cells reported low efficiencies of 0.53% and 0.95%, both of which suffered from low fill factors and low current densities,<sup>402,408</sup> while  $\text{AgBiS}_2$  QDs have also been seen to improve on Pt as a contact material.<sup>409</sup> Recent work by Bernechea *et al.* however, using tetramethylammonium iodide-treated  $\text{AgBiS}_2$  nanocrystals in a p–i–n junction between PTB7 and ZnO, has recently given a record cell of 6.3% efficiency, equaling many of the record antimony and bismuth-based cells, with a high  $J_{\text{sc}}$  of  $22 \text{ mA cm}^{-2}$  and FF of 0.63.<sup>410</sup> A relatively low  $V_{\text{oc}}$  of 0.45 eV was attributed to trap-assisted recombination, and so improvements in synthesis could easily lead to significantly easier charge transport and even higher efficiencies in the future.

Also notable is the recent production of a cell based on cubic  $\text{AgBi}_2\text{I}_7$ , a compound that has only been sparsely characterised previously.<sup>411</sup> Sargent and co-workers investigated the  $\text{AgI–BiI}_3$  solid solution, producing a thin film of  $\text{AgBi}_2\text{I}_7$ , and reporting a direct band gap of 1.86 eV.<sup>412</sup> A subsequent nanocomposite cell, with  $\text{AgBi}_2\text{I}_7$  between mesoporous  $\text{TiO}_2$  and P3HT, gave an efficiency of 1.12%, with a high fill factor of 0.67, but limited by relatively lower current density and voltage. As with many of the above compounds, further attention could lead to significant improvements in the future.

### 7.5 Cesium and hybrid bismuth iodides

The cesium bismuth iodide  $\text{Cs}_3\text{Bi}_2\text{I}_9$  and its methylammonium counterpart,  $(\text{CH}_3\text{NH}_3)_3\text{Bi}_2\text{I}_9$ , have come under attention similar to the antimony analogue. While past studies have performed detailed study concerning the low temperature ( $\sim 200 \text{ K}$ ) ferro-elastic phase transition of  $\text{Cs}_3\text{Bi}_2\text{I}_9$ ,<sup>413–415</sup> and the vibrational

properties of  $(\text{CH}_3\text{NH}_3)_3\text{Bi}_2\text{I}_9$ ,<sup>416</sup> thorough electronic characterization of the room temperature phases has only been performed recently. This structural behaviour may still be relevant, however, given that exciton–phonon coupling in the bromide analogue,  $\text{Cs}_3\text{Bi}_2\text{Br}_9$ , has been shown to lead to a much stronger exciton binding energy than the lead halide perovskites.<sup>417</sup> Unlike the layered  $\text{Cs}_3\text{Sb}_2\text{I}_9$ , the bismuth compounds occupy the ‘zero dimensional’  $\text{Cs}_3\text{Cr}_2\text{Cl}_9$  structure, with isolated  $[\text{Bi}_2\text{I}_9]^{3-}$  dimers of face-sharing octahedra surrounded by the free  $\text{Cs}^+$  or  $(\text{CH}_3\text{NH}_3)^+$  cations,<sup>418–420</sup> raising the possibility of lower carrier mobilities. Indeed, Lehner *et al.*'s theoretical and experimental characterisation of  $\text{Cs}_3\text{Bi}_2\text{I}_9$  found much lower band dispersion in comparison with MAPI, indicative of low mobilities, together with a relatively high indirect optical band gap of 1.9 eV (Fig. 8d).<sup>349</sup> Nevertheless,  $\text{Cs}_3\text{Bi}_2\text{I}_9$  was used as an absorber on mesoporous  $\text{TiO}_2$  by Park *et al.* to give a best cell with 1% efficiency and a  $V_{\text{oc}}$  of 0.85 eV,<sup>421</sup> a significant improvement on the equivalent  $(\text{CH}_3\text{NH}_3)_3\text{Bi}_2\text{I}_9$  cells which had efficiencies below 0.2% and much lower  $V_{\text{oc}}$  and  $J_{\text{sc}}$ . Other attempts to use  $(\text{CH}_3\text{NH}_3)_3\text{Bi}_2\text{I}_9$  since, with alternate organic hole transporting layers, have seen small improvements in  $J_{\text{sc}}$ <sup>422,423</sup> and fill factor,<sup>424</sup> but efficiencies remain low, despite a similar band gap of 2.1 eV and strong absorption.<sup>425,426</sup> Buonassisi and co-workers also studied the photoluminescence behaviour of  $(\text{CH}_3\text{NH}_3)_3\text{Bi}_2\text{I}_9$ , finding a decay time of 760 ps—up to  $10^3$  lower than the highest recombination lifetime in MAPI films, however it is noted that a  $<1 \text{ ns}$  lifetime is comparable to the initial values recorded for popular absorbers such as  $\text{Cu}_2\text{ZnSnSe}_4$  and  $\text{SnS}$ .<sup>425</sup> A low PL quantum efficiency of 0.4% was also recorded and attributed to non-radiative recombination pathways; Park *et al.* found defect states in the XPS of  $\text{Cs}_3\text{Bi}_2\text{I}_9$  that suggest it may be similarly limited.<sup>421</sup> It is evident that the photovoltaic behaviour of both materials may be enhanced if further work to reduce the impact of these pathways is performed, and, as both studies also found that the bismuth iodides were stable in air over a month, these compounds do present a potential avenue for hybrid bismuth PV materials.

$(\text{CH}_3\text{NH}_3)_3\text{Bi}_2\text{I}_9$  is not the only inorganic–organic bismuth iodide to have been examined for photovoltaic activity, with the one-dimensional hexanediammonium bismuth iodide,  $(\text{H}_3\text{NC}_6\text{H}_{12}\text{NH}_3)\text{BiI}_5$ , recently trialled in a mesoporous  $\text{TiO}_2$  architecture. Like the bismuth iodides above, these devices also possessed low  $V_{\text{oc}}$  and  $J_{\text{sc}}$ , and a band gap close to 2 eV, however they also showed greater film coverage and thermal stability than MAPI.<sup>429</sup>

### 7.6 Double perovskites (elpasolites)

Very recently, there have been significant efforts to move beyond the  $\text{A}^1\text{M}^{\text{II}}\text{X}_3$  perovskite formula to the double perovskite  $\text{A}^1_2\text{M}^{\text{I}}\text{M}^{\text{III}}\text{X}_6$ . Crucially, this allows the expansion of the perovskite motif beyond Group 14 ions on the M site while retaining the successful 3D perovskite structure (Fig. 9a). While double perovskites in the oxide family are well known as fuel cells,<sup>433,434</sup> only a few relevant halides such as  $\text{Cs}_2\text{NaBiCl}_6$ , with absorption much higher in energy than the ideal photovoltaic range, are known.<sup>435,436</sup> In 2015, however, Giorgi and Yamashita





**Fig. 9** (a) Crystal structure of  $\text{Cs}_2\text{BiAgBr}_6$ . Adapted with permission from ref. 427. Copyright 2015, American Chemical Society. (b) Time-resolved room temperature photoluminescence (PL) of single-crystal and powder  $\text{Cs}_2\text{BiAgBr}_6$ , including fits for the PL decay time ( $\tau$ ). Reprinted with permission from ref. 428. Copyright 2016, American Chemical Society.

proposed a simple substitution of  $\text{Tl}^+$  and  $\text{Bi}^{3+}$ , in place of  $\text{Pb}^{2+}$ , into the tetragonal MAPI structure using DFT, finding a theoretical bandgap of 1.68 eV, compared with MAPI's 1.62 eV using the PBE functional.<sup>437</sup> However, as the authors admit, Tl presents an environmental risk and its possible replacement by its neighbour In<sup>I</sup> would likely lead to instability issues, similar to  $\text{Sn}^{\text{II}}$ .

Instead, at the beginning of 2016, multiple separate groups have published on the  $\text{Cs}_2\text{AgBiX}_6$  family. Slavney *et al.* synthesised  $\text{Cs}_2\text{AgBiBr}_6$  and discuss its photoluminescence behaviour, finding a long decay time of 660 ns which is attributed to a long recombination lifetime dominated by non-radiative recombination, similar to that found in MAPI, and estimating the indirect band gap at 1.95 eV (Fig. 9b).<sup>428</sup> McClure *et al.* were able to synthesise both the bromide and chloride, finding indirect bandgaps of 2.19 eV and 2.77 eV respectively from diffuse reflectance spectroscopy and supporting these observations with DFT calculations, finding hole effective masses slightly lower than those in the analogous methylammonium lead bromide.<sup>452</sup> Additionally, both studies examined the stability of these materials: Slavney *et al.* found the bromide stable up to 430 °C and no evidence of degradation under either moisture or light after 30 days, however, while McClure *et al.* found no significant decomposition in the chloride, the reflectance and XRD pattern of  $\text{Cs}_2\text{AgBiBr}_6$  was observed to degrade when stored in light and air. Volonakis *et al.* have performed a wider theoretical screening of the double perovskites using hybrid DFT, examining  $\text{M}^{\text{I}} = \text{Cu}$ , Ag, Au and  $\text{M}^{\text{III}} = \text{Bi}$ , Sb and additionally synthesising  $\text{Cs}_2\text{BiAgCl}_6$  to support their observations.<sup>427</sup> Of those predicted, a linear decrease is observed in all cases down the halide group, while, for  $\text{M}^{\text{I}}$ , the Ag compounds have higher band gaps, and Au the lowest; as such,  $\text{Cs}_2\text{AgSbI}_6$ ,  $\text{Cs}_2\text{BiCuI}_6$  and  $\text{Cs}_2\text{BiAuBr}_6$  are those observed to have band gaps within the optimal 1.0–1.5 eV range. Further work from the Giustino group has seen the accurate prediction of the band gaps of  $\text{Cs}_2\text{BiAgCl}_6$  and  $\text{Cs}_2\text{AgBiBr}_6$  using quasiparticle GW theory.<sup>453</sup> Recent work by the Cheetham and co-workers has seen the synthesis of the methylammonium double perovskites  $(\text{MA})_2\text{KBiCl}_6$  and  $(\text{MA})_2\text{TlBiBr}_6$ : however,  $(\text{MA})_2\text{KBiCl}_6$ 's indirect band gap of 3.04 eV is too high for efficient use in photovoltaics, and while the 2.16 eV bandgap of  $(\text{MA})_2\text{TlBiBr}_6$  is direct, the inclusion of toxic thallium, as

discussed above, would minimize the benefit of removing lead.<sup>454,455</sup> It is clear that while the double perovskite motif allows the replacement of Pb, their wide, indirect band gaps and the potential issue of stability may be problematic for further PV applications.

This split-ion approach for producing bismuth double-perovskites has similarly been proposed on the anion site, with a mix of chalcogenides and halides: DFT calculations predicted the hypothetical  $\text{CH}_3\text{NH}_3\text{BiSI}_2$  to have a similar band gap, dielectric behaviour and effective masses to MAPI.<sup>456</sup> However, another wide-ranging theoretical study on the analogous inorganic  $\text{AM}(\text{Ch}^{\text{II}}\text{X}^{\text{I}})_3$  ( $\text{A} = \text{Cs}$ , Ba,  $\text{M} = \text{Sb}$ , Bi, Ch = O, S, Se, Te and X = F, Cl, Br, I) compounds has found that all were unstable to decomposition, and the authors' attempts to synthesise these compounds found no evidence that the target phases were produced.<sup>28</sup> As Hong *et al.* reflect, it is clear that when such alternatives, particularly quaternary compounds with a larger number of competing phases, are predicted, assessments of their stability should not be neglected.

### 7.7 Further inorganic–organic bismuth compounds

Further to those previously mentioned, there exists a massive library of extant hybrid inorganic–organic bismuth and anti-mony compounds due to the surge in interest in the 1990's and early 2000's. Several reduced dimensionality bismuth iodides exist, yet are relatively under-characterised: these include guanidinium, iodoformamidinium and a variety of alkyl and photoactive-cation bismuth iodides, many of which were synthesised by David Mitzi and his co-workers.<sup>100,103,317,457–461</sup> Indeed, there are still many new bismuth compounds being discovered even this year,<sup>462</sup> some of which may already be promising PV candidate materials.<sup>463,464</sup> Given the diversity of coordination, dimensionality and organic character in these examples alone, it is clear there already exists a wide parameter space of potential inorganic–organic bismuth compounds. A full survey of these materials is beyond the scope of this review, yet a number of excellent reviews cover this section of bismuth chemistry already, particularly low-dimensionality structures.<sup>71,465,466</sup> Nevertheless, the field of hybrid-organic bismuth compounds would appear to open up an opportunity: a new frontier of non-toxic, optoelectronic materials waiting to be examined and explored by the photovoltaic community.

## 8 Outlook and conclusion

Table 1 gives the highest recorded efficiencies and device specifications for all  $ns^2$  solar absorbers discussed in this Review. Lead-based devices currently outperform all alternatives—this is, in part, due to the enormous research effort these materials have experienced but also to the excellent properties of lead, highlighted in our introduction. Despite the similarities in the electronic properties of the group 14 metals and the long-standing research interest in tin solar absorbers, tin-based devices still lag behind their lead counterparts. This can be attributed the sensitivity of  $\text{Sn}^{2+}$  (and similarly,  $\text{Ge}^{2+}$ ) to





**Table 1** Highest recorded efficiencies for a range of  $ns^2$  solar absorbers, with corresponding device open-circuit voltage ( $V_{oc}$ ), short-circuit current ( $J_{sc}$ ), fill factor (FF), band gap ( $E_g$ ), and fabrication details. Nanocomposite devices are those containing mesoporous  $TiO_2$  (m- $TiO_2$ ) impregnated with absorber material. SILAR and ALD refer to the successive ionic layer adsorption and reaction, and atomic layer deposition processes, respectively

Absorber	PCE (%)	$V_{oc}$ (V)	$J_{sc}$ (mA cm <sup>-2</sup> )	FF (%)	$E_g$ (eV)	Architecture	Cell type	Deposition method	Ref.	
<b>Pb</b>	$CH_3NH_3PbI_3$	19.1	1.09	22.4	80	FTO/c- $TiO_2$ /m- $TiO_2$ /perovskite/spiro-OMeTAD/Au	Nanocomposite	Spin coating	430	
	(MA,FA,Cs) $PbI_3$	21.1 <sup>a</sup>	1.15	23.5	78	FTO/c- $TiO_2$ /mp- $TiO_2$ /perovskite/spiro-OMeTAD/Au	Nanocomposite	Spin coating	431	
	$CH(NH_2)_2PbI_3$	20.1	1.06	24.7	78	FTO/NiO/perovskite/PCBM/LiF/Al	Planar heterojunction	Spin coating	432	
	$CsPbI_3$	2.9	0.80	12.0	—	FTO/c- $TiO_2$ /perovskite/spiro-OMeTAD	Planar heterojunction	Spin coating	80	
	$CsPbI_2Br$	9.8	1.10	11.89	75	FTO/c- $TiO_2$ /perovskite/spiro-OMeTAD/Ag	Planar heterojunction	Spin coating	79	
	$FA_{0.83}Cs_{0.17}Pb(I_{0.6}Br_{0.4})_3$	17.9	1.09	19.4	79	FTO/SnO <sub>2</sub> /PCBM/perovskite/spiro-OMeTAD/Ag	Planar heterojunction	Spin coating	89	
	(PEA) <sub>2</sub> (MA) <sub>50</sub> Pb <sub>60</sub> I <sub>81</sub>	15.4	1.09	19.1	74	FTO/c- $TiO_2$ /perovskite/spiro-OMeTAD/Au	Planar heterojunction	Spin coating	110	
	( $CH_3NH_3$ ) <sub>2</sub> Pb(SCN) <sub>2</sub> I <sub>2</sub>	8.3	0.87	15.1	63	FTO/c- $TiO_2$ /perovskite/spiro-OMeTAD/Au	Planar heterojunction	Spin coating	120	
	PbS	9.2	0.54	30.0	58	FTO/ $TiO_2$ /PbS/MoO <sub>3</sub> /Au/Ag	Quantum dot	Spin coating	148	
	PbSe	6.2	0.52	23.4	52	ITO/ $TiO_2$ /PbSe/MoO <sub>3</sub> /Al	Quantum dot	Spin coating	157	
<b>Sn</b>	$CH_3NH_3SnI_3$	6.4	0.88	16.8	42	FTO/c- $TiO_2$ /mp- $TiO_2$ /perovskite/spiro-OMeTAD/Au	Nanocomposite	Spin coating	173	
	$CH(NH_2)_2SnI_3$	4.8	0.32	23.7	63	FTO/c- $TiO_2$ /mp- $TiO_2$ /perovskite/spiro-OMeTAD/Au	Nanocomposite	Spin coating	164	
	$CsSnI_3$	2.0	0.24	22.7	37	FTO/c- $TiO_2$ /mp- $TiO_2$ /perovskite/m-MTDATA/Au	Nanocomposite	Spin coating	181	
	SnS	4.4	0.37	20.2	58	ITO/ZnO/Zn(O,S) <sub>2</sub> N/SnS/Mo	Planar heterojunction	ALD	193	
	$CsGeI_3$	3.2	0.53	10.5	53	FTO/ $TiO_2$ /perovskite/P3HT/Au	Planar heterojunction	Spin coating	239	
<b>Ge</b>	$CH_3NH_3GeI_3$	0.2	0.15	4.0	30	FTO/c- $TiO_2$ /mp- $TiO_2$ /perovskite/spiro-OMeTAD/Au	Nanocomposite	Spin coating	238	
	<b>Sb</b>	$Sb_2S_3$	7.5	0.71	16.1	65	FTO/ $TiO_2$ /mp- $TiO_2$ /Sb <sub>2</sub> S <sub>3</sub> /PCPDTBT/PEDOT:PSS/Au	Nanocomposite	Spin coating	266
$Sb_2Se_3$		5.6	0.40	25.1	57	FTO/CdS/Sb <sub>2</sub> Se <sub>3</sub> /Au	Planar heterojunction	Spin coating	243	
$Sb_2S_3-xSe_x$		6.6	0.48	24.9	56	FTO/ $TiO_2$ /mp- $TiO_2$ /absorber/P3HT/Au	Nanocomposite	Spin coating	292	
$CuSbS_2$		3.2	0.47	15.6	44	Al/n-ZnO/i-ZnO/CdS/CuSbS <sub>2</sub> /Mo	Planar heterojunction	Spin coating	308	
$CuSbSe_2$		3.5	0.35	22.8	—	MgF/Ni:Al/n-ZnO/i-ZnO/CdS/CuSbSe <sub>2</sub> /Mo	Planar heterojunction	DC sputtering	310	
(MA) <sub>3</sub> Sb <sub>2</sub> I <sub>9</sub>		0.5	0.89	1.0	55	ITO/PEDOT:PSS/(MA) <sub>3</sub> Sb <sub>2</sub> I <sub>9</sub> /PC61BM/nano-ZnO/Al	Planar heterojunction	Spin coating	316	
$Cs_3Sb_2I_9$		<1.0	0.31	—	—	FTO/c- $TiO_2$ /Cs <sub>3</sub> Sb <sub>2</sub> I <sub>9</sub> /PTAA/Au	Planar heterojunction	Co-evaporation	313	
<b>Bi</b>		$Bi_2S_3$	2.5	0.50	9.3	54	FTO/ $TiO_2$ /CdS/ $Bi_2S_3$ /ZnS	Quantum dot	SILAR	333
		$Bi_2S_3$ /P3HT	3.3	0.69	10.7	45	ITO/ $TiO_2$ / $Bi_2S_3$ /P3HT/MoO <sub>3</sub> /Au	Planar heterojunction	Spin coating	346
		$Bi_2S_3$ /PbS QD	4.9	0.40	24.2	50	ITO/PbS QD/PbS/ $Bi_2S_3$ /Ag	Bulk nano-heterojunction	Spin coating	338
	$BiI_3$	0.3	0.42	1.7	45	FTO/ $TiO_2$ / $BiI_3$ /PTAA/Au	Planar heterojunction	Spin coating	350	
	$BiSI$	<0.1	0.39	0.1	40	FTO/ $BiSI$ /p-CuSCN/FTO/Pt	Planar heterojunction	Spray pyrolysis	369	
	$BiOI$	1.0	0.61	3.8	45	FTO/ $TiO_2$ / $BiOI$ ( $I_3^-/I^-$ )/FTO/Pt	Liquid electrolyte	SILAR	380	
	$AgBiS_2$	6.3	0.45	22.1	63	ITO/ZnO/Ag $BiS_2$ /PTB7/Ag	Planar heterojunction	Hot injection	410	
	$AgBi_2I_7$	1.2	0.56	3.3	67	FTO/c- $TiO_2$ /mp- $TiO_2$ /Ag $Bi_2I_7$ /P3HT/Au	Nanocomposite	Spin coating	412	
	$Cs_3Bi_2I_9$	1.1	0.85	2.2	60	FTO/ $TiO_2$ /mp- $TiO_2$ /perovskite/spiro-OMeTAD/Ag	Planar heterojunction	Spin coating	421	
	( $CH_3NH_3$ ) <sub>3</sub> $Bi_2I_6$ ( $H_3NC_6H_{12}NH_3$ ) $BiI_5$	0.1 <0.1	0.68 0.40	0.5 0.1	33 43	FTO/ $TiO_2$ /mp- $TiO_2$ /perovskite/spiro-OMeTAD/Ag FTO/c- $TiO_2$ /mp- $TiO_2$ /absorber/spiroOMeTAD/Au	Planar heterojunction Nanocomposite	Spin coating Spin coating	421 429	

<sup>a</sup> The highest recorded efficiency for a hybrid halide lead perovskite solar cell is 22.1%, however, only limited technical specifications for this device have been released.<sup>467</sup> As such, we report details for the next highest efficiency device here.



**Fig. 10** Efficiency improvements over time for a range of  $ns^2$  solar absorbers. Only materials with greater than one recorded device efficiency improvement are included. Devices with efficiencies lower than 0.1% have been omitted. Lead-based absorbers (orange): hybrid perovskite ref. 86, 184, 431, 432 and 438–442; inorganic perovskite ref. 79, 80, 443 and 444; layered perovskite ref. 96, 110 and 120; PbS ref. 147, 148 and 445–451. Tin-based absorbers (green): hybrid perovskite ref. 172 and 173; inorganic perovskite ref. 180 and 181; SnS ref. 192, 193, 200 and 224. Antimony-based absorbers (blue): Sb<sub>2</sub>S<sub>3</sub> ref. 260–262, 265, 266 and 278; Sb<sub>2</sub>Se<sub>3</sub> ref. 243, 278, 285, 288 and 289; Sb<sub>2</sub>S<sub>3-x</sub>Se<sub>x</sub> ref. 291 and 292; CuSbS<sub>2</sub> ref. 306 and 308. Bismuth-based absorbers (red): MA<sub>3</sub>Bi<sub>2</sub>I<sub>9</sub> ref. 421 and 422; Bi<sub>2</sub>S<sub>3</sub> ref. 333, 344 and 346; AgBiS<sub>2</sub> ref. 402, 408 and 410; BiOI ref. 379 and 380.

oxidation, which hampers device fabrication and leads to efficiency losses. It is therefore essential that alternative schemes to stabilise tin-based devices are developed. Antimony devices have seen persistent improvements to their efficiencies since 2009 and show the second highest performance of any material behind lead. Their earth-abundant composition make them attractive as emerging solar absorbers and with increased attention, efficiencies should continue to rise. Analogously, there has been an increase in reports of bismuth-based devices over the last few years, spurred on by its non-toxic nature and ideal electronic properties, which are expected to be ideal for solar cell applications. As can be seen in Fig. 10, bismuth containing absorbers have recently begun to show efficiencies comparable with the best antimony and tin alternatives.

Several materials highlighted in this review show excellent promise as solar absorbers. The layered lead hybrid perovskites have seen a sharp rise in efficiency in recent months—comparable with the rise of MAPI—due to the development of a “quasi-2D” structure. This approach combines the beneficial increase in stability seen in the purely layered structures, with the excellent optical and electronic properties possessed by the 3D perovskites. In this way, stability and optical properties can be finely tuned to enable moisture tolerant devices with exceptional absorber characteristics. The bismuth containing material AgBiS<sub>2</sub> has also seen rapid advances in efficiencies recently. Its 3D-connected cubic structure draws parallels with the hybrid perovskites and should allow for comparable charge transport properties.

The rise of the hybrid perovskites and emergence of MAPI has galvanised the photovoltaic community with a renewed focus. That an unknown and little studied material can overtake all other third-generation solar absorbers in such a short number of years firmly demonstrates the potential of an earth-abundant and cost-effective alternative to silicon technologies. Such a dramatic rise in efficiencies has relied on a multi-disciplinary approach and has brought together a decade’s worth of advancements in the photonics, engineering and synthetic chemistry communities. Nonetheless, MAPI clearly possesses a fortuitous combination of properties that make it tolerant of a wide range of synthesis conditions and an ideal solar absorber. For this reason, the rise of MAPI should be seen as an outlier and not a precedent to be expected of all emerging absorbers. Instead, it is likely that the next generation of solar materials will require many years of development and optimisation before they can reach comparable efficiencies. Regardless, the emergent field of  $ns^2$  solar absorbers shows particular promise for the future of photovoltaic energy generation.

## Acknowledgements

DOS acknowledges support from the SUPERSOLAR Solar Energy Hub (EP/J017361/1) for the provision of a flexible funding call award, EPSRC (EP/N01572X/1), and membership of the Materials Design Network. CNS is grateful to the Department of Chemistry at UCL for the provision of a DTA studentship, and AMG



acknowledges Diamond Light Source for the co-sponsorship of a studentship on the EPSRC Centre for Doctoral Training in Molecular Modelling and Materials Science (EP/L015862/1). We would also like to acknowledge T. Gershon, A. Zakutayev, T. D. Veal, A. Walsh, R. Seshadri, R. G. Palgrave, T. Buonassisi, R. L. Z. Hoye, V. Steinmann, R. E. Brandt, P. K. Nair, B. C. Melot, S. Chen, D. B. Mitzi, T. K. Cheetham, H. J. Snaith, S. Lany, E. Arca, Y. Yan, H. Bronstein, J. D. Major, K. Durose, K. T. Butler, J. M. Frost, C. H. Hendon, J. M. Skelton, B. A. D. Williamson, A. J. Jackson, J. Buckeridge, S.-H. Wei, M. Van Schilfhaarde, C. Persson, F. Giustino, and P. M. Woodward for many illuminating discussions at conferences and the myriad of fascinating contributions they have published in this field.

## References

- N. S. Lewis and D. G. Nocera, *Proc. Natl. Acad. Sci. U. S. A.*, 2006, **103**, 15729–15735.
- W. A. Hermann, *Energy*, 2006, **31**, 1685–1702.
- J. Nelson, *The physics of solar cells*, World Scientific, 2003, vol. 57.
- J. Ondraczek, N. Komendantova and A. Patt, *Renewable Energy*, 2015, **75**, 888–898.
- J. Peng, L. Lu and H. Yang, *Renewable Sustainable Energy Rev.*, 2013, **19**, 255–274.
- W. Shockley and H. J. Queisser, *J. Appl. Phys.*, 1961, **32**, 510–519.
- C. Wadia, A. P. Alivisatos and D. M. Kammen, *Environ. Sci. Technol.*, 2009, **43**, 2072–2077.
- N. G. Dhere, *Sol. Energy Mater. Sol. Cells*, 2007, **91**, 1376–1382.
- M. A. Green, A. Ho-Baillie and H. J. Snaith, *Nat. Photonics*, 2014, **8**, 506–514.
- M. Grätzel, *Nat. Mater.*, 2014, **13**, 838–842.
- T. Baikie, Y. Fang, J. M. Kadro, M. Schreyer, F. Wei, S. G. Mhaisalkar, M. Graetzel and T. J. White, *J. Mater. Chem. A*, 2013, **1**, 5628–5641.
- V. D'Innocenzo, G. Grancini, M. J. Alcocer, A. R. S. Kandada, S. D. Stranks, M. M. Lee, G. Lanzani, H. J. Snaith and A. Petrozza, *Nat. Commun.*, 2014, **5**, 3586.
- A. Walsh, D. O. Scanlon, S. Chen, X. G. Gong and S.-H. Wei, *Angew. Chem.*, 2015, **127**, 1811–1814.
- Y. Deng, E. Peng, Y. Shao, Z. Xiao, Q. Dong and J. Huang, *Energy Environ. Sci.*, 2015, **8**, 1544–1550.
- G. Xing, N. Mathews, S. Sun, S. S. Lim, Y. M. Lam, M. Gratzel, S. Mhaisalkar and T. C. Sum, *Science*, 2013, **342**, 344–347.
- Y. Shao, Z. Xiao, C. Bi, Y. Yuan and J. Huang, *Nat. Commun.*, 2014, **5**, 5784.
- C. Wehrenfennig, G. E. Eperon, M. B. Johnston, H. J. Snaith and L. M. Herz, *Adv. Mater.*, 2014, **26**, 1584–1589.
- Y. Zhao and K. Zhu, *J. Phys. Chem. Lett.*, 2013, **4**, 2880–2884.
- A. T. Barrows, A. J. Pearson, C. K. Kwak, A. D. F. Dunbar, A. R. Buckley and D. G. Lidzey, *Energy Environ. Sci.*, 2014, **7**, 2944.
- D. S. Bhachu, D. O. Scanlon, E. J. Saban, H. Bronstein, I. P. Parkin, C. J. Carmalt and R. G. Palgrave, *J. Mater. Chem. A*, 2015, **3**, 8970–8980.
- G. Hodes and D. Cahen, *Nat. Photonics*, 2014, **8**, 87–88.
- J. A. Christians, J. S. Manser and P. V. Kamat, *J. Phys. Chem. Lett.*, 2015, **6**, 852–857.
- G. Nagabhushana, R. Shivaramaiah and A. Navrotsky, *Proc. Natl. Acad. Sci. U. S. A.*, 2016, **113**, 7717–7721.
- S. Guarnera, A. Abate, W. Zhang, J. M. Foster, G. Richardson, A. Petrozza and H. J. Snaith, *J. Phys. Chem. Lett.*, 2015, **6**, 432–437.
- G. Niu, X. Guo and L. Wang, *J. Mater. Chem. A*, 2015, **3**, 8970–8980.
- J. Yang and T. L. Kelly, *Inorg. Chem.*, 2016, DOI: acs.inorgchem.6b01307.
- T. J. Jacobsson, J.-P. Correa-Baena, M. Pazoki, M. Saliba, K. Schenk, M. Grätzel and A. Hagfeldt, *Energy Environ. Sci.*, 2016, **9**, 1706–1724.
- F. Hong, B. Saparov, W. Meng, Z. Xiao, D. B. Mitzi and Y. Yan, *J. Phys. Chem. C*, 2016, **120**, 6435–6441.
- S. Körbel, M. A. Marques and S. Botti, *J. Mater. Chem. C*, 2016, **4**, 3157–3167.
- J. Berry, T. Buonassisi, D. A. Egger, G. Hodes, L. Kronik, Y.-L. Loo, I. Lubomirsky, S. R. Marder, Y. Mastai and J. S. Miller, *Adv. Mater.*, 2015, **27**, 5102–5112.
- P. P. Boix, S. Agarwala, T. M. Koh, N. Mathews and S. G. Mhaisalkar, *J. Phys. Chem. Lett.*, 2015, **6**, 898–907.
- K. Gregor, S. Shijing and K. C. Anthony, *Chem. Sci.*, 2014, **5**, 4712–4715.
- G. Kieslich, S. Sun and T. Cheetham, *Chem. Sci.*, 2015, **6**, 3430–3433.
- W. Travis, E. Glover, H. Bronstein, D. Scanlon and R. Palgrave, *Chem. Sci.*, 2016, **7**, 4548–4556.
- T. C. Sum and N. Mathews, *Energy Environ. Sci.*, 2014, **7**, 2518–2534.
- C. C. Stoumpos and M. G. Kanatzidis, *Adv. Mater.*, 2016, **28**, 5778–5793.
- R. E. Brandt, V. Stevanović, D. S. Ginley and T. Buonassisi, *MRS Commun.*, 2015, **5**, 265–275.
- J. M. Frost, K. T. Butler, F. Brivio, C. H. Hendon, M. van Schilfhaarde and A. Walsh, *Nano Lett.*, 2014, **14**, 2584–2590.
- P. Umari, E. Mosconi and F. De Angelis, *Sci. Rep.*, 2014, **4**, 4467.
- L. Yu and A. Zunger, *Phys. Rev. Lett.*, 2012, **108**, 068701.
- A. B. Kehoe, D. O. Scanlon and G. W. Watson, *Phys. Rev. B: Condens. Matter Mater. Phys.*, 2011, **83**, 3–6.
- A. M. Ganose and D. O. Scanlon, *J. Mater. Chem. C*, 2016, **4**, 1467–1475.
- S. De Wolf, J. Holovsky, S.-J. Moon, P. Löper, B. Niesen, M. Ledinsky, F.-J. Haug, J.-H. Yum and C. Ballif, *J. Phys. Chem. Lett.*, 2014, **5**, 1035–1039.
- A. Zakutayev, C. M. Caskey, A. N. Fioretti, D. S. Ginley, J. Vidal, V. Stevanovic, E. Tea and S. Lany, *J. Phys. Chem. Lett.*, 2014, **5**, 1117–1125.
- P. Azarhoosh, J. M. Frost, S. McKechnie, A. Walsh and M. van Schilfhaarde, *APL Mater.*, 2016, **4**, 091501.
- J. Mattheis, J. H. Werner and U. Rau, *Phys. Rev. B: Condens. Matter Mater. Phys.*, 2008, **77**, 085203.
- R. Jaramillo, M.-J. Sher, B. K. Ofori-Oakai, V. Steinmann, C. Yang, K. Hartman, K. A. Nelson, A. M. Lindenberg, R. G. Gordon and T. Buonassisi, *J. Appl. Phys.*, 2016, **119**, 035101.
- S. D. Stranks, G. E. Eperon, G. Grancini, C. Menelaou, M. J. P. Alcocer, T. Leijtens, L. M. Herz, A. Petrozza and H. J. Snaith, *Science*, 2013, **342**, 341–344.
- A. E. Maughan, A. M. Ganose, M. M. Bordelon, E. M. Miller, D. O. Scanlon and J. R. Neilson, *J. Am. Chem. Soc.*, 2016, **138**, 8453–8464.
- R. H. Bube, *Photoelectronic Properties of Semiconductors*, Cambridge University Press, 1992.
- Y. Kutes, L. Ye, Y. Zhou, S. Pang, B. D. Huey and N. P. Padture, *J. Phys. Chem. Lett.*, 2014, **5**, 3335–3339.
- S. Liu, F. Zheng, N. Z. Koocher, H. Takenaka, F. Wang and A. M. Rappe, *J. Phys. Chem. Lett.*, 2015, **6**, 693–699.
- J. Beilsten-Edmands, G. E. Eperon, R. D. Johnson, H. J. Snaith and P. G. Radaelli, *Appl. Phys. Lett.*, 2015, **106**, 173502.
- K. T. Butler, J. M. Frost and A. Walsh, *Energy Environ. Sci.*, 2015, **8**, 838–848.
- M. Kepenekian, R. Robles, C. Katan, D. Saporì, L. Pedesseau and J. Even, *ACS Nano*, 2015, **9**, 11557–11567.
- T. Etienne, E. Mosconi and F. D. Angelis, *J. Phys. Chem. Lett.*, 2016, **7**, 1638–1645.
- L. Yu, R. S. Kokenyesi, D. A. Keszler and A. Zunger, *Adv. Energy Mater.*, 2013, **3**, 43–48.
- K. Leo, *Nat. Nanotechnol.*, 2015, **10**, 574–575.
- B. Hailegnaw, S. Kirmayer, E. Edri, G. Hodes and D. Cahen, *J. Phys. Chem. Lett.*, 2015, **6**, 1543–1547.
- K. K. Bass, R. E. McAnally, S. Zhou, P. I. Djurovich, M. E. Thompson and B. C. Melot, *Chem. Commun.*, 2014, **50**, 15819–15822.
- E. Mosconi, J. M. Azzipiroz and F. De Angelis, *Chem. Mater.*, 2015, **27**, 4885–4892.
- J. A. Christians, J. S. Manser and P. V. Kamat, *J. Phys. Chem. Lett.*, 2015, **6**, 2086–2095.
- D. Bryant, N. Aristidou, S. Pont, I. Sanchez-Molina, T. Chotchunangatchaval, S. Wheeler, J. R. Durrant and S. A. Haque, *Energy Environ. Sci.*, 2016, **9**, 1655–1660.
- B. Conings, J. Drijkoningen, N. Gauquelin, A. Babayigit, J. D'Haen, L. D'Olieslaeger, A. Ethirajan, J. Verbeeck, J. Manca, E. Mosconi, F. D. Angelis and H.-G. Boyen, *Adv. Energy Mater.*, 2015, **5**, 1500477.
- E. J. Juarez-Perez, Z. Hawash, S. R. Raga, L. K. Ono and Y. Qi, *Energy Environ. Sci.*, 2016, DOI: 10.1039/C6EE02016J.
- A. Pisoni, J. Jaćimović, O. S. Barišić, M. Spina, R. Gaál, L. Forró and E. Horváth, *J. Phys. Chem. Lett.*, 2014, **5**, 2488–2492.
- Y.-Y. Zhang, S. Chen, P. Xu, H. Xiang, X.-G. Gong, A. Walsh and S.-H. Wei, *arXiv:1506.01301 [cond-mat.mtrl-sci]*, 2015.
- A. M. Ganose, C. N. Savory and D. O. Scanlon, *J. Phys. Chem. Lett.*, 2015, **6**, 4594–4598.



- 69 S. N. Habisreutinger, D. P. McMeekin, H. J. Snaith and R. J. Nicholas, *APL Mater.*, 2016, **4**, 091503.
- 70 D. B. Mitzi, *J. Chem. Soc., Dalton Trans.*, 2001, 1–12.
- 71 B. Saparov and D. B. Mitzi, *Chem. Rev.*, 2016, **116**, 4558–4596.
- 72 A. Amat, E. Mosconi, E. Ronca, C. Quarti, P. Umari, M. K. Nazeeruddin, M. Grätzel and F. De Angelis, *Nano Lett.*, 2014, **14**, 3608–3616.
- 73 G. E. Eperon, S. D. Stranks, C. Menelaou, M. B. Johnston, L. M. Herz and H. J. Snaith, *Energy Environ. Sci.*, 2014, **7**, 982–988.
- 74 C. C. Stoumpos, C. D. Malliakas and M. G. Kanatzidis, *Inorg. Chem.*, 2013, **52**, 9019–9038.
- 75 M. T. Weller, O. J. Weber, J. M. Frost and A. Walsh, *J. Phys. Chem. Lett.*, 2015, **6**, 3209–3212.
- 76 A. Binek, F. C. Hanusch, P. Docampo and T. Bein, *J. Phys. Chem. Lett.*, 2015, **6**, 1249–1253.
- 77 N. Pellet, P. Gao, G. Gregori, T.-Y. Yang, M. K. Nazeeruddin, J. Maier and M. Grätzel, *Angew. Chem., Int. Ed.*, 2014, **53**, 3151–3157.
- 78 J. Brgoch, A. Lehner, M. Chabinye and R. Seshadri, *J. Phys. Chem. C*, 2014, **118**, 27721–27727.
- 79 R. J. Sutton, G. E. Eperon, L. Miranda, E. S. Parrott, B. A. Kamino, J. B. Patel, M. T. Hörantner, M. B. Johnston, A. A. Haghighirad, D. T. Moore and H. J. Snaith, *Adv. Energy Mater.*, 2016, **6**, 1502458.
- 80 G. E. Eperon, G. M. Paterno, R. J. Sutton, A. Zampetti, A. A. Haghighirad, F. Cacialli and H. J. Snaith, *J. Mater. Chem. A*, 2015, **3**, 19688–19695.
- 81 L. Protesescu, S. Yakunin, M. I. Bodnarchuk, F. Krieg, R. Caputo, C. H. Hendon, R. X. Yang, A. Walsh and M. V. Kovalenko, *Nano Lett.*, 2015, **15**, 3692–3696.
- 82 K. T. Butler, J. M. Frost and A. Walsh, *Mater. Horiz.*, 2015, **2**, 228–231.
- 83 Y. Tidhar, E. Edri, H. Weissman, D. Zohar, G. Hodes, D. Cahen, B. Rybtchinski and S. Kirmayer, *J. Am. Chem. Soc.*, 2014, **136**, 13249–13256.
- 84 N. Yantara, Y. Fang, S. Chen, H. A. Dewi, P. P. Boix, S. G. Mhaisalkar and N. Mathews, *Chem. Mater.*, 2015, **27**, 2309–2314.
- 85 J. H. Noh, S. H. Im, J. H. Heo, T. N. Mandal and S. I. Seok, *Nano Lett.*, 2013, **13**, 1764–1769.
- 86 N. J. Jeon, J. H. Noh, Y. C. Kim, W. S. Yang, S. Ryu and S. I. Seok, *Nat. Mater.*, 2014, **13**, 897–903.
- 87 W. Rehman, R. L. Milot, G. E. Eperon, C. Wehrenfennig, J. L. Boland, H. J. Snaith, M. B. Johnston and L. M. Herz, *Adv. Mater.*, 2015, **27**, 7938–7944.
- 88 F. Brivio, C. Caetano and A. Walsh, *J. Phys. Chem. Lett.*, 2016, **7**, 1083–1087.
- 89 D. P. McMeekin, G. Sadoughi, W. Rehman, G. E. Eperon, M. Saliba, M. T. Hörantner, A. Haghighirad, N. Sakai, L. Korte, B. Rech, M. B. Johnston, L. M. Herz and H. J. Snaith, *Science*, 2016, **351**, 151–155.
- 90 A. Walsh, *J. Mater. Chem. C*, 2015, **119**, 5755–5760.
- 91 D. Uneyama, Y. Lin and H. I. Karunadasa, *Chem. Mater.*, 2016, **28**, 3241–3244.
- 92 T. M. Koh, K. Thirumal, H. S. Soo and N. Mathews, *ChemSusChem*, 2016, **9**, 2541–2558.
- 93 D. B. Mitzi, C. D. Dimitrakopoulos and L. L. Kosbar, *Chem. Mater.*, 2001, **13**, 3728–3740.
- 94 D. B. Mitzi, K. Chondroudis and C. R. Kagan, *IBM J. Res. Dev.*, 2001, **45**, 29–45.
- 95 D. B. Mitzi, D. R. Medeiros and P. R. L. Malenfant, *Inorg. Chem.*, 2002, **41**, 2134–2145.
- 96 L. N. Quan, M. Yuan, R. Comin, O. Voznyy, E. M. Beauregard, S. Hoogland, A. Buin, A. R. Kirmani, K. Zhao, A. Amassian, D. H. Kim and E. H. Sargent, *J. Am. Chem. Soc.*, 2016, **138**, 2649–2655.
- 97 W. Jiang, J. Ying, W. Zhou, K. Shen, X. Liu, X. Gao, F. Guo, Y. Gao and T. Yang, *Chem. Phys. Lett.*, 2016, **658**, 71–75.
- 98 D. B. Mitzi, C. A. Feild, W. T. A. Harrison and A. M. Guloy, *Nature*, 1994, **369**, 467–469.
- 99 D. B. Mitzi, in *Progress in Inorganic Chemistry*, ed. K. D. Karlin, John Wiley & Sons Inc., 1999, ch. 1, vol. 48, pp. 1–121.
- 100 S. Wang, D. B. Mitzi, C. A. Feild and A. Guloy, *J. Am. Chem. Soc.*, 1995, **117**, 5297–5302.
- 101 D. B. Mitzi, *Chem. Mater.*, 1996, **8**, 791–800.
- 102 K. Chondroudis and D. B. Mitzi, *Chem. Mater.*, 1999, **11**, 3028–3030.
- 103 D. B. Mitzi, *Inorg. Chem.*, 2000, **39**, 6107–6113.
- 104 D. B. Mitzi, *Chem. Mater.*, 2001, **13**, 3283–3298.
- 105 N. Kitazawa and Y. Watanabe, *J. Phys. Chem. Solids*, 2010, **71**, 797–802.
- 106 T. Ishihara, J. Takahashi and T. Goto, *Phys. Rev. B: Condens. Matter Mater. Phys.*, 1990, **42**, 11099–11107.
- 107 E. A. Muljarov, S. G. Tikhodeev, N. A. Gippius and T. Ishihara, *Phys. Rev. B: Condens. Matter Mater. Phys.*, 1995, **51**, 14370–14378.
- 108 N. Mercier, S. Poiroux, A. Riou and P. Batail, *Inorg. Chem.*, 2004, **43**, 8361–8366.
- 109 S. Sourisseau, N. Louvain, W. Bi, N. Mercier, D. Rondeau, F. Boucher, J.-Y. Buzaré and C. Legein, *Chem. Mater.*, 2007, **19**, 600–607.
- 110 I. C. Smith, E. T. Hoke, D. Solis-Ibarra, M. D. McGehee and H. I. Karunadasa, *Angew. Chem., Int. Ed.*, 2014, **53**, 11232–11235.
- 111 D. H. Cao, C. C. Stoumpos, O. K. Farha, J. T. Hupp and M. G. Kanatzidis, *J. Am. Chem. Soc.*, 2015, **137**, 7843–7850.
- 112 Z. Yang, C.-C. Chueh, F. Zuo, J. H. Kim, P.-W. Liang and A. K.-Y. Jen, *Adv. Energy Mater.*, 2015, **5**, 1500328.
- 113 A. Dualeh, P. Gao, S. I. Seok, M. K. Nazeeruddin and M. Grätzel, *Chem. Mater.*, 2014, **26**, 6160–6164.
- 114 J. A. Christians, P. A. M. Herrera and P. V. Kamat, *J. Am. Chem. Soc.*, 2015, **137**, 1530–1538.
- 115 H. Tsai, W. Nie, J.-C. Blancon, C. C. Stoumpos, R. Asadpour, B. Harutyunyan, A. J. Neukirch, R. Verduzco, J. J. Crochet, S. Tretiak, L. Pedesseau, J. Even, M. A. Alam, G. Gupta, J. Lou, P. M. Ajayan, M. J. Bedzyk, M. G. Kanatzidis and A. D. Mohite, *Nature*, 2016, **536**, 312–316.
- 116 A. Halder, R. Chulliyil, A. S. Subbiah, T. Khan, S. Chattoraj, A. Chowdhury and S. K. Sarkar, *J. Phys. Chem. Lett.*, 2015, **6**, 3483–3489.
- 117 W. Ke, C. Xiao, C. Wang, B. Saparov, H.-S. Duan, D. Zhao, Z. Xiao, P. Schulz, S. P. Harvey, W. Liao, W. Meng, Y. Yu, A. J. Cimaroli, C.-S. Jiang, K. Zhu, M. Al-Jassim, G. Fang, D. B. Mitzi and Y. Yan, *Adv. Mater.*, 2016, **28**, 5214–5221.
- 118 Y. Iwade, K. Kawamura, K. Igarashi and J. Mochinaga, *J. Phys. Chem.*, 1982, **86**, 5205–5208.
- 119 Y. Chen, B. Li, W. Huang, D. Gao and Z. Liang, *Chem. Commun.*, 2015, **51**, 11997–11999.
- 120 Q. Jiang, D. Rebollar, J. Gong, E. L. Piacentino, C. Zheng and T. Xu, *Angew. Chem., Int. Ed.*, 2015, **54**, 7617–7620.
- 121 M. Daub and H. Hillebrecht, *Angew. Chem., Int. Ed.*, 2015, **54**, 11016–11017.
- 122 Z. Xiao, W. Meng, B. Saparov, H.-S. Duan, C. Wang, C. Feng, W.-Q. Liao, W. Ke, D. Zhao, J. Wang, D. B. Mitzi and Y. Yan, *J. Phys. Chem. Lett.*, 2016, **7**, 1213–1218.
- 123 G. A. Mousdis, V. Gionis, G. C. Papavassiliou, C. P. Raptopoulou and A. Terzis, *J. Mater. Chem.*, 1998, **8**, 2259–2262.
- 124 H.-B. Duan, H.-R. Zhao, X.-M. Ren, H. Zhou, Z.-F. Tian and W.-Q. Jin, *Dalton Trans.*, 2011, **40**, 1672–1683.
- 125 S.-P. Zhao and X.-M. Ren, *Dalton Trans.*, 2011, **40**, 8261–8272.
- 126 G.-E. Wang, X.-M. Jiang, M.-J. Zhang, H.-F. Chen, B.-W. Liu, M.-S. Wang and G.-C. Guo, *CrystEngComm*, 2013, **15**, 10399.
- 127 H. A. Evans, A. J. Lehner, J. G. Labram, D. H. Fabini, O. Barreda, S. R. Smock, G. Wu, M. L. Chabinye, R. Seshadri and F. Wudl, *Chem. Mater.*, 2016, **28**, 3607–3611.
- 128 A. E. Maughan, J. A. Kurzman and J. R. Neilson, *Inorg. Chem.*, 2015, **54**, 370–378.
- 129 D. H. Fabini, J. G. Labram, A. J. Lehner, J. S. Bechtel, H. A. Evans, A. Van der Ven, F. Wudl, M. L. Chabinye and R. Seshadri, *Inorg. Chem.*, 2016, DOI: acs.inorgchem.6b01539.
- 130 B. R. Vincent, K. N. Robertson, T. S. Cameron and O. Knop, *Can. J. Chem.*, 1987, **65**, 1042–1046.
- 131 K. Pradeesh, M. Agarwal, K. K. Rao and G. V. Prakash, *Solid State Sci.*, 2010, **12**, 95–98.
- 132 E. M. Kosower, *J. Org. Chem.*, 1964, **29**, 956–957.
- 133 W. V. E. Doering and L. H. Knox, *J. Am. Chem. Soc.*, 1957, **79**, 352–356.
- 134 J.-J. Liu, Y.-F. Guan, C. Jiao, M.-J. Lin, C.-C. Huang and W. Dai, *Dalton Trans.*, 2015, **44**, 5957–5960.
- 135 C. N. Savory, R. G. Palgrave, H. Bronstein and D. O. Scanlon, *Sci. Rep.*, 2016, **6**, 20626.
- 136 H. Bronstein, J. M. Frost, A. Hadipour, Y. Kim, C. B. Nielsen, R. S. Ashraf, B. P. Rand, S. Watkins and I. McCulloch, *Chem. Mater.*, 2013, **25**, 277–285.
- 137 W. Travis, C. E. Knapp, C. N. Savory, A. M. Ganose, P. Kafourou, X. Song, Z. Sharif, J. K. Cockcroft, D. O. Scanlon, H. Bronstein and R. G. Palgrave, *Inorg. Chem.*, 2016, **55**, 3393–3400.
- 138 Z. Ning, X. Gong, R. Comin, G. Walters, F. Fan, O. Voznyy, E. Yassitepe, A. Buin, S. Hoogland and E. H. Sargent, *Nature*, 2015, **523**, 324–328.





- 208 M. Ristov, G. Sinadinovski, I. Grozdanov and M. Mitreski, *Thin Solid Films*, 1989, **173**, 53–58.
- 209 M. T. S. Nair and P. K. Nair, *Semicond. Sci. Technol.*, 1991, **6**, 132.
- 210 H.-Y. He, J. Fei and J. Lu, *Mater. Sci. Semicond. Process.*, 2014, **24**, 90–95.
- 211 J. Y. Kim and S. M. George, *J. Mater. Chem. C*, 2010, **114**, 17597–17603.
- 212 P. Sinsermsuksakul, J. Heo, W. Noh, A. S. Hock and R. G. Gordon, *Adv. Energy Mater.*, 2011, **1**, 1116–1125.
- 213 N. K. Reddy and K. R. Reddy, *Thin Solid Films*, 1998, **325**, 4–6.
- 214 B. Thangaraju and P. Kaliannan, *J. Phys. D: Appl. Phys.*, 2000, **33**, 1054.
- 215 S. Dhanapandian, A. G. Manohari, C. Manoharan, K. S. Kumar and T. Mahalingam, *Mater. Sci. Semicond. Process.*, 2014, **18**, 65–70.
- 216 K. Deraman, S. Sakrani, B. Ismatl, Y. Wahab and R. Gould, *Int. J. Electron.*, 1994, **76**, 917–922.
- 217 M. Devika, N. K. Reddy, K. Ramesh, R. Ganesan, K. Gunasekar, E. Gopal and K. R. Reddy, *J. Electrochem. Soc.*, 2007, **154**, H67–H73.
- 218 A. Wangperawong, S. M. Herron, R. R. Runser, C. Hägglund, J. T. Tanskanen, B. M. Clemens and S. F. Bent, *Appl. Phys. Lett.*, 2013, **103**, 052105.
- 219 A. Ghazali, Z. Zainal, M. Z. Hussein and A. Kassim, *Sol. Energy Mater. Sol. Cells*, 1998, **55**, 237–249.
- 220 L. Cheng, M. Liu, M. Wang, S. Wang, G. Wang, Q. Zhou and Z. Chen, *J. Alloys Compd.*, 2012, **545**, 122–129.
- 221 S. Zimin, E. Gorlachev, I. Amirov, V. Naumov, G. Dubov, V. Gremenok and S. Bashkirov, *Semicond. Sci. Technol.*, 2013, **29**, 015009.
- 222 T. Sajeesh, A. R. Warriar, C. S. Kartha and K. Vijayakumar, *Thin Solid Films*, 2010, **518**, 4370–4374.
- 223 H. H. Park, R. Heasley, L. Sun, V. Steinmann, R. Jaramillo, K. Hartman, R. Chakraborty, P. Sinsermsuksakul, D. Chua and T. Buonassisi, *Prog. Photovoltaics*, 2015, **23**, 901–908.
- 224 P. Sinsermsuksakul, K. Hartman, S. B. Kim, J. Heo, L. Sun, H. H. Park, R. Chakraborty, T. Buonassisi and R. G. Gordon, *Appl. Phys. Lett.*, 2013, **102**, 053901.
- 225 L. A. Burton and A. Walsh, *Appl. Phys. Lett.*, 2013, **102**, 132111.
- 226 M. Patel and A. Ray, *ACS Appl. Mater. Interfaces*, 2014, **6**, 10099–10106.
- 227 C. Gao, H. Shen and L. Sun, *Appl. Surf. Sci.*, 2011, **257**, 6750–6755.
- 228 P. K. Nair, A. R. Garcia-Angelmo and M. T. S. Nair, *Phys. Status Solidi A*, 2015, **177**, 170–177.
- 229 A. Rabkin, S. Samuha, R. E. Abutbul, V. Ezersky, L. Meshi and Y. Golan, *Nano Lett.*, 2015, **15**, 2174–2179.
- 230 P. K. Nair, E. Barrios-Salgado and M. T. S. Nair, *Phys. Status Solidi A*, 2016, **8**, 2229–2236.
- 231 G. Rosenfeld and E. Wallace, *Arch. Ind. Hyg. Occup. Med.*, 1953, **8**, 466–479.
- 232 Q. Gu, Q. Pan, X. Wu, W. Shi and C. Fang, *J. Cryst. Growth*, 2000, **212**, 605–607.
- 233 G. QingTian, P. QiWei, S. Wei, S. Xun and F. ChangShui, *Prog. Cryst. Growth Charact. Mater.*, 2000, **40**, 89–95.
- 234 L.-C. Tang, C.-S. Chang and J. Y. Huang, *J. Phys.: Condens. Matter*, 2000, **12**, 9129.
- 235 L. C. Tang, J. Y. Huang, C. Chang, M. Lee and L. Liu, *J. Phys.: Condens. Matter*, 2005, **17**, 7275.
- 236 D.-K. Seo, N. Gupta, M.-H. Whangbo, H. Hillebrecht and G. Thiele, *Inorg. Chem.*, 1998, **37**, 407–410.
- 237 L.-C. Tang, Y.-C. Chang, J.-Y. Huang, M.-H. Lee and C.-S. Chang, *Jpn. J. Appl. Phys.*, 2009, **48**, 112402.
- 238 T. Krishnamoorthy, H. Ding, C. Yan, W. L. Leong, T. Baikie, Z. Zhang, M. Sherburne, S. Li, M. Asta, N. Mathews and S. G. Mhaisalkar, *J. Mater. Chem. A*, 2015, **3**, 23829–23832.
- 239 C. Huang, X. C. Yan, G. Cui, Z. Liu, S. Pang and H. Xu, *Novel germanium-containing perovskite material and solar cell comprising same*, CN Pat. App. CN 201410173750, 2014.
- 240 C. C. Stoumpos, L. Frazer, D. J. Clark, Y. S. Kim, S. H. Rhim, A. J. Freeman, J. B. Ketterson, J. I. Jang and M. G. Kanatzidis, *J. Am. Chem. Soc.*, 2015, **137**, 6804–6819.
- 241 B. D. Malone and E. Kaxiras, *Phys. Rev. B: Condens. Matter Mater. Phys.*, 2013, **87**, 245312.
- 242 Y.-Q. Zhao, L.-J. Wu, B. Liu, L.-Z. Wang, P.-B. He and M.-Q. Cai, *J. Power Sources*, 2016, **313**, 96–103.
- 243 Y. Zhou, L. Wang, S. Chen, S. Qin, X. Liu, J. Chen, D.-J. Xue, M. Luo, Y. Cao, Y. Cheng, E. H. Sargent and J. Tang, *Nat. Photonics*, 2015, **9**, 409–415.
- 244 L. Makinistian and E. Albanesi, *J. Phys.: Condens. Matter*, 2007, **19**, 186211.
- 245 D. D. Vaughn, R. J. Patel, M. A. Hickner and R. E. Schaak, *J. Am. Chem. Soc.*, 2010, **132**, 15170–15172.
- 246 P. D. Antunez, J. J. Buckley and R. L. Brutchey, *Nanoscale*, 2011, **3**, 2399.
- 247 L. Makinistian and E. A. Albanesi, *Phys. Rev. B: Condens. Matter Mater. Phys.*, 2006, **74**, 045206.
- 248 L. Makinistian and E. Albanesi, *Comput. Mater. Sci.*, 2011, **50**, 2872–2879.
- 249 K. N. Abrikosov, V. Bankina, L. Poretskaya, L. Shelimova and E. Skudnova, *Semiconducting II-VI, IV-VI and V-VI Compounds*, Plenum Press, NY, 1969, vol. 249, p. 14.
- 250 A. Stanchev and C. Vodenicharov, *Thin Solid Films*, 1976, **38**, 67–72.
- 251 S. Hao, F. Shi, V. Dravid, M. Kanatzidis and C. Wolverton, *Chem. Mater.*, 2016, **28**, 3218–3226.
- 252 S. Sundar and J. Chakravarty, *Int. J. Environ. Res. Public Health*, 2010, **7**, 4267–4277.
- 253 B. Yang, L. Wang, J. Han, Y. Zhou, H. Song, S. Chen, J. Zhong, L. Lv, D. Niu and J. Tang, *Chem. Mater.*, 2014, **26**, 3135–3143.
- 254 A. Kyono, M. Kimata, M. Matsuhisa, Y. Miyashita and K. Okamoto, *Phys. Chem. Miner.*, 2002, **29**, 254–260.
- 255 N. W. Tidswell, F. H. Kruse and J. D. McCullough, *Acta Crystallogr.*, 1957, **10**, 99–102.
- 256 J. Curran, R. Philippe, J. Joseph and A. Gagnaire, *Chem. Phys. Lett.*, 1982, **89**, 511–515.
- 257 O. Savadogo and K. C. Mandal, *J. Electrochem. Soc.*, 1992, **139**, L16–L18.
- 258 O. Savadogo and K. C. Mandal, *J. Electrochem. Soc.*, 1994, **141**, 2871–2877.
- 259 O. Savadogo and K. C. Mandal, *J. Phys. D: Appl. Phys.*, 1994, **27**, 1070.
- 260 Y. Itzhaik, O. Niitsoo, M. Page and G. Hodes, *J. Phys. Chem. C*, 2009, **113**, 4254–4256.
- 261 J. A. Chang, J. H. Rhee, S. H. Im, Y. H. Lee, H. Jung Kim, S. I. Seok, M. K. Nazeeruddin and M. Grätzel, *Nano Lett.*, 2010, **10**, 2609–2612.
- 262 S.-J. Moon, Y. Itzhaik, J.-H. Yum, S. M. Zakeeruddin, G. Hodes and M. Grätzel, *J. Phys. Chem. Lett.*, 2010, **1**, 1524–1527.
- 263 A. M. Huerta-Flores, N. A. García-Gómez, S. M. de la Parra-Arciniega and E. M. Sánchez, *Semicond. Sci. Technol.*, 2016, **31**, 085011.
- 264 K. Tsujimoto, D.-C. Nguyen, S. Ito, H. Nishino, H. Matsuyoshi, A. Konno, G. R. A. Kumara and K. Tennakone, *J. Phys. Chem. C*, 2012, **116**, 13465–13471.
- 265 J. A. Chang, S. H. Im, Y. H. Lee, H.-J. Kim, C.-S. Lim, J. H. Heo and S. I. Seok, *Nano Lett.*, 2012, **12**, 1863–1867.
- 266 Y. C. Choi, D. U. Lee, J. H. Noh, E. K. Kim and S. I. Seok, *Adv. Funct. Mater.*, 2014, **24**, 3587–3592.
- 267 Y. C. Choi and S. I. Seok, *Adv. Funct. Mater.*, 2015, **25**, 2892–2898.
- 268 V. Janošević, M. Mitrić, N. Bundaleski, Z. Rakočević and I. L. Validžić, *Prog. Photovoltaics*, 2015, **24**, 704–715.
- 269 M. Y. Versavel and J. A. Haber, *Thin Solid Films*, 2007, **515**, 7171–7176.
- 270 R. Mane and C. Lokhande, *Mater. Chem. Phys.*, 2003, **82**, 347–354.
- 271 I. Grozdanov, *Semicond. Sci. Technol.*, 1994, **9**, 1234.
- 272 K. C. Godel, Y. C. Choi, B. Roose, A. Sadhanala, H. J. Snaith, S. I. Seok, U. Steiner and S. K. Pathak, *Chem. Commun.*, 2015, **51**, 8640–8643.
- 273 R. X. Yang, K. T. Butler and A. Walsh, *J. Phys. Chem. Lett.*, 2015, **6**, 5009–5014.
- 274 T. B. Nasr, H. Maghraoui-Meherzi, H. B. Abdallah and R. Bennaceur, *Phys. B*, 2011, **406**, 287–292.
- 275 R. Caracas and X. Gonze, *Phys. Chem. Miner.*, 2005, **32**, 295–300.
- 276 M. R. Filip, C. E. Patrick and F. Giustino, *Phys. Rev. B: Condens. Matter Mater. Phys.*, 2013, **87**, 205125.
- 277 J. Ma, Y. Wang, Y. Wang, P. Peng, J. Lian, X. Duan, Z. Liu, X. Liu, Q. Chen, T. Kim, G. Yao and W. Zheng, *CrystEngComm*, 2011, **13**, 2369–2374.
- 278 K. Rajpure and C. Bhosale, *Mater. Chem. Phys.*, 2002, **73**, 6–12.
- 279 Y. Lai, Z. Chen, C. Han, L. Jiang, F. Liu, J. Li and Y. Liu, *Appl. Surf. Sci.*, 2012, **261**, 510–514.
- 280 C. Chen, W. Li, Y. Zhou, C. Chen, M. Luo, X. Liu, K. Zeng, B. Yang, C. Zhang, J. Han and J. Tang, *Appl. Phys. Lett.*, 2015, **107**, 043905.
- 281 J. Yang, Y. Lai, Y. Fan, Y. Jiang, D. Tang, L. Jiang, F. Liu and J. Li, *RSC Adv.*, 2015, **5**, 85592–85597.





- 355 M. Ruck, *Z. Kristallogr.*, 1995, **210**, 650–655.
- 356 D. J. Singh, *Phys. Rev. B: Condens. Matter Mater. Phys.*, 2010, **82**, 155145.
- 357 G. E. Jellison, J. O. Ramey and L. A. Boatner, *Phys. Rev. B: Condens. Matter Mater. Phys.*, 1999, **59**, 9718–9721.
- 358 N. J. Podraza, W. Qiu, B. B. Hinojosa, H. Xu, M. A. Motyka, S. R. Phillpot, J. E. Baciak, S. Trolier-McKinstry and J. C. Nino, *J. Appl. Phys.*, 2013, **114**, 033110.
- 359 H. Yorikawa and S. Muramatsu, *J. Phys.: Condens. Matter*, 2008, **20**, 325220.
- 360 R. E. Brandt, R. C. Kurchin, R. L. Z. Hoye, J. R. Poindexter, M. W. B. Wilson, S. Sulekar, F. Lenahan, P. X. T. Yen, V. Stevanović, J. C. Nino, M. G. Bawendi and T. Buonassisi, *J. Phys. Chem. Lett.*, 2015, **6**, 4297–4302.
- 361 F. Ma, M. Zhou, Y. Jiao, G. Gao, Y. Gu, A. Bilic, Z. Chen and A. Du, *Sci. Rep.*, 2015, **5**, 17558.
- 362 E. Dönges, *Z. Anorg. Allg. Chem.*, 1950, **263**, 112–132.
- 363 W. Haase-Wessel, *Naturwissenschaften*, 1973, **60**, 474.
- 364 T. P. Braun and F. J. DiSalvo, *Acta Crystallogr., Sect. C: Cryst. Struct. Commun.*, 2000, **56**, e1–e2.
- 365 D.-W. Shin, S.-C. Hyun, S. an Park, Y.-G. Kim, C. dae Kim and W.-T. Kim, *J. Phys. Chem. Solids*, 1994, **55**, 825–830.
- 366 R. Nitsche and W. Merz, *J. Phys. Chem. Solids*, 1960, **13**, 154–155.
- 367 J. Horák and K. Čermák, *Czechoslovakij fyziceskij zurnal B*, 1965, **15**, 536–538.
- 368 N. T. Hahn, J. L. Self and C. B. Mullins, *J. Phys. Chem. Lett.*, 2012, **3**, 1571–1576.
- 369 N. T. Hahn, A. J. E. Rettie, S. K. Beal, R. R. Fullon and C. B. Mullins, *J. Phys. Chem. C*, 2012, **116**, 24878–24886.
- 370 H. Shi, W. Ming and M.-H. Du, *Phys. Rev. B: Condens. Matter Mater. Phys.*, 2016, **93**, 104108.
- 371 K.-L. Zhang, C.-M. Liu, F.-Q. Huang, C. Zheng and W.-D. Wang, *Appl. Catal., B*, 2006, **68**, 125–129.
- 372 J. Zhang, F. Shi, J. Lin, D. Chen, J. Gao, Z. Huang, X. Ding and C. Tang, *Chem. Mater.*, 2008, **20**, 2937–2941.
- 373 H. Cheng, B. Huang and Y. Dai, *Nanoscale*, 2014, **6**, 2009–2026.
- 374 D. S. Bhachu, S. J. A. Moniz, S. Sathasivam, D. O. Scanlon, A. Walsh, S. M. Bawaked, M. Mokhtar, A. Y. Obaid, I. P. Parkin, J. Tang and C. J. Carmalt, *Chem. Sci.*, 2016, **7**, 4832–4841.
- 375 A. M. Ganose, M. Cuff, K. T. Butler, A. Walsh and D. O. Scanlon, *Chem. Mater.*, 2016, **28**, 1980–1984.
- 376 L. Zhao, X. Zhang, C. Fan, Z. Liang and P. Han, *Phys. B*, 2012, **407**, 3364–3370.
- 377 S. Poznyak and A. Kulak, *Electrochim. Acta*, 1990, **35**, 1941–1947.
- 378 K. Zhao, X. Zhang and L. Zhang, *Electrochem. Commun.*, 2009, **11**, 612–615.
- 379 K. Wang, F. Jia, Z. Zheng and L. Zhang, *Electrochem. Commun.*, 2010, **12**, 1764–1767.
- 380 S. Sfaelou, D. Raptis, V. Dracopoulos and P. Lianos, *RSC Adv.*, 2015, **5**, 95813–95816.
- 381 M. Fang, H. Jia, W. He, Y. Lei, L. Zhang and Z. Zheng, *Phys. Chem. Chem. Phys.*, 2015, **17**, 13531–13538.
- 382 A. Luz, J. Conradt, M. Wolff, H. Kalt and C. Feldmann, *Solid State Sci.*, 2013, **19**, 172–177.
- 383 D. J. Temple, A. B. Kehoe, J. P. Allen, G. W. Watson and D. O. Scanlon, *J. Phys. Chem. C*, 2012, **116**, 7334–7340.
- 384 M. Kumar and C. Persson, *J. Renewable Sustainable Energy*, 2013, **5**, 031616.
- 385 D. Parker and D. J. Singh, *Phys. Rev. B: Condens. Matter Mater. Phys.*, 2011, **83**, 233206.
- 386 C. Tablero, *J. Phys. Chem. C*, 2015, **119**, 8857–8863.
- 387 S. H. Pawar, A. J. Pawar and P. N. Bhosale, *Bull. Mater. Sci.*, 1986, **8**, 423–426.
- 388 P. Sonawane, P. Wani, L. Patil and T. Seth, *Mater. Chem. Phys.*, 2004, **84**, 221–227.
- 389 V. Balasubramanian, N. Suriyanarayanan, S. Prabakar, S. Srikanth and P. Ravi, *Optoelectron. Adv. Mater., Rapid Commun.*, 2012, **6**, 104–106.
- 390 W. Wubet, D.-H. Kuo and H. Abdullah, *J. Solid State Chem.*, 2015, **230**, 237–242.
- 391 V. Estrella, M. T. S. Nair and P. K. Nair, *Semicond. Sci. Technol.*, 2003, **18**, 190.
- 392 N. J. Gerein and J. A. Haber, *Chem. Mater.*, 2006, **18**, 6297–6302.
- 393 F. Mesa, A. Dussan and G. Gordillo, *Phys. B*, 2009, **404**, 5227–5230.
- 394 F. Mesa, G. Gordillo, T. Dittrich, K. Ellmer, R. Baier and S. Sadewasser, *Appl. Phys. Lett.*, 2010, **96**, 082113.
- 395 M. Yakushev, P. Maiello, T. Raadik, M. Shaw, P. Edwards, J. Krustok, A. Mudryi, I. Forbes and R. Martin, *Thin Solid Films*, 2014, **562**, 195–199.
- 396 A. B. Kehoe, D. J. Temple, G. W. Watson and D. O. Scanlon, *Phys. Chem. Chem. Phys.*, 2013, **15**, 15477–15484.
- 397 M. Kumar and C. Persson, *Appl. Phys. Lett.*, 2013, **102**, 062109.
- 398 C. Tablero, *Prog. Photovoltaics*, 2013, **21**, 894–899.
- 399 J. Yin and J. Jia, *CrystEngComm*, 2014, **16**, 2795–2801.
- 400 X. Liu, H. Zheng, J. Zhang, Y. Xiao and Z. Wang, *J. Mater. Chem. A*, 2013, **1**, 10703–10712.
- 401 S. Geller and J. H. Wernick, *Acta Crystallogr.*, 1959, **12**, 46–54.
- 402 P.-C. Huang, W.-C. Yang and M.-W. Lee, *J. Phys. Chem. C*, 2013, **117**, 18308–18314.
- 403 K. Hoang, S. D. Mahanti, J. R. Salvador and M. G. Kanatzidis, *Phys. Rev. Lett.*, 2007, **99**, 156403.
- 404 S. N. Guin, S. Banerjee, D. Sanyal, S. K. Pati and K. Biswas, *Inorg. Chem.*, 2016, **55**, 6323–6331.
- 405 B. Pejova, I. Grozdanov, D. Nesheva and A. Petrova, *Chem. Mater.*, 2008, **20**, 2551–2565.
- 406 B. Pejova, D. Nesheva, Z. Aneva and A. Petrova, *J. Phys. Chem. C*, 2011, **115**, 37–46.
- 407 C. Chen, X. Qiu, S. Ji, C. Jia and C. Ye, *CrystEngComm*, 2013, **15**, 7644–7648.
- 408 S. Zhou, J. Yang, W. Li, Q. Jiang, Y. Luo, D. Zhang, Z. Zhou and X. Li, *J. Electrochem. Soc.*, 2016, **163**, D63–D67.
- 409 N. Liang, W. Chen, F. Dai, X. Wu, W. Zhang, Z. Li, J. Shen, S. Huang, Q. He, J. Zai, N. Fang and X. Qian, *CrystEngComm*, 2015, **17**, 1902–1905.
- 410 M. Bernechea, N. C. Miller, G. Xercavins, D. So, A. Stavrinadis and G. Konstantatos, *Nat. Photonics*, 2016, **10**, 521–525.
- 411 P. Fourcroy, M. Palazzi, J. Rivet, J. Flahaut and R. Céolin, *Mater. Res. Bull.*, 1979, **14**, 325–328.
- 412 Y. Kim, Z. Yang, A. Jain, O. Voznyy, G.-H. Kim, M. Liu, L. N. Quan, F. P. Garcia de Arquer, R. Comin, J. Z. Fan and E. H. Sargent, *Angew. Chem., Int. Ed.*, 2016, **55**, 9586.
- 413 S. V. Mel'nikova and A. I. Zaitsev, *Phys. Solid State*, 1997, **39**, 1652–1654.
- 414 A. Jorio, R. Currat, D. Myles, G. McIntyre, I. Aleksandrova, J. Kiat and P. Saint-Gregoire, *Phys. Rev. B: Condens. Matter Mater. Phys.*, 2000, **61**, 3857–3862.
- 415 F. V. Motsnyi, O. M. Smolanka, V. I. Sugakov and E. Y. Peresh, *Solid State Commun.*, 2006, **137**, 221–224.
- 416 G. Bator, J. Baran, R. Jakubas and L. Sobczyk, *J. Mol. Struct.*, 1998, **450**, 89–100.
- 417 K. K. Bass, L. Estergreen, C. N. Savory, J. Buckeridge, D. O. Scanlon, P. I. Djurovich, S. E. Bradforth, M. E. Thompson and B. C. Melot, *Inorg. Chem.*, 2016, DOI: 10.1021/acs.inorgchem.6b01571.
- 418 O. Lindquist, *Acta Chem. Scand.*, 1968, **22**, 2943–2952.
- 419 B. Chabot and E. Parthé, *Acta Crystallogr., Sect. B: Struct. Sci.*, 1978, **34**, 645–648.
- 420 K. Eckhardt, V. Bon, J. Getzschmann, J. Grothe, F. M. Wisser and S. Kaskel, *Chem. Commun.*, 2016, **52**, 3058–3060.
- 421 B.-W. Park, B. Philippe, X. Zhang, H. Rensmo, G. Boschloo and E. M. J. Johansson, *Adv. Mater.*, 2015, **27**, 6806–6813.
- 422 M. Lyu, J.-H. Yun, M. Cai, Y. Jiao, P. V. Bernhardt, M. Zhang, Q. Wang, A. Du, H. Wang, G. Liu and L. Wang, *Nano Res.*, 2016, **9**, 692–702.
- 423 T. Singh, A. Kulkarni, M. Ikegami and T. Miyasaka, *ACS Appl. Mater. Interfaces*, 2016, **8**, 14542–14547.
- 424 S. Öz, J.-C. Hebig, E. Jung, T. Singh, A. Lepcha, S. Olthof, F. Jan, Y. Gao, R. German, P. H. van Loosdrecht, K. Meerholz, T. Kirchartz and S. Mathur, *Sol. Energy Mater. Sol. Cells*, 2016, DOI: 10.1016/j.solmat.2016.01.035.
- 425 R. L. Z. Hoye, R. E. Brandt, A. Oshero, V. Stevanović, S. D. Stranks, M. W. B. Wilson, H. Kim, A. J. Akey, J. D. Perkins, R. C. Kurchin, J. R. Poindexter, E. N. Wang, M. G. Bawendi, V. Bulović and T. Buonassisi, *Chem. – Eur. J.*, 2016, **22**, 2605–2610.
- 426 T. Kawai and S. Shimanuki, *Phys. Status Solidi B*, 1993, **177**, K43–K45.
- 427 G. Volonakis, M. R. Filip, A. A. Haghghirad, N. Sakai, B. Wenger, H. J. Snaith and F. Giustino, *J. Phys. Chem. Lett.*, 2016, **7**, 1254–1259.
- 428 A. H. Slavney, T. Hu, A. M. Lindenberg and H. I. Karunadasa, *J. Am. Chem. Soc.*, 2016, **138**, 2138–2141.



- 429 D. M. Fabian and S. Ardo, *J. Mater. Chem. A*, 2016, **4**, 6837–6841.
- 430 C. Roldan-Carmona, P. Gratia, I. Zimmermann, G. Grancini, P. Gao, M. Graetzel and M. K. Nazeeruddin, *Energy Environ. Sci.*, 2015, **8**, 3550–3556.
- 431 M. Saliba, T. Matsui, J.-Y. Seo, K. Domanski, J.-P. Correa-Baena, M. K. Nazeeruddin, S. M. Zakeeruddin, W. Tress, A. Abate, A. Hagfeldt and M. Grätzel, *Energy Environ. Sci.*, 2016, **9**, 1989–1997.
- 432 W. S. Yang, J. H. Noh, N. J. Jeon, Y. C. Kim, S. Ryu, J. Seo and S. I. Seok, *Science*, 2015, **348**, 1234–1237.
- 433 Y.-H. Huang, R. I. Dass, Z.-L. Xing and J. B. Goodenough, *Science*, 2006, **312**, 254–257.
- 434 S. Sengodan, S. Choi, A. Jun, T. H. Shin, Y.-W. Ju, H. Y. Jeong, J. Shin, J. T. S. Irvine and G. Kim, *Nat. Mater.*, 2015, **14**, 205–209.
- 435 L. R. Morris and W. R. Robinson, *Acta Crystallogr., Sect. B: Struct. Sci.*, 1972, **28**, 653–654.
- 436 F. Pelle, B. Jacquier, J. Denis and B. Blanzat, *J. Lumin.*, 1978, **17**, 61–72.
- 437 G. Giorgi and K. Yamashita, *Chem. Lett.*, 2015, **44**, 826–828.
- 438 A. Kojima, K. Teshima, Y. Shirai and T. Miyasaka, *J. Am. Chem. Soc.*, 2009, **131**, 6050–6051.
- 439 J.-H. Im, C.-R. Lee, J.-W. Lee, S.-W. Park and N.-G. Park, *Nanoscale*, 2011, **3**, 4088–4093.
- 440 J. Burschka, N. Pellet, S.-J. Moon, R. Humphry-Baker, P. Gao, M. K. Nazeeruddin and M. Grätzel, *Nature*, 2013, **499**, 316–319.
- 441 J. H. Heo, H. J. Han, D. Kim, T. K. Ahn and S. H. Im, *Energy Environ. Sci.*, 2015, **8**, 1602–1608.
- 442 Q. Dong, Y. Yuan, Y. Shao, Y. Fang, Q. Wang and J. Huang, *Energy Environ. Sci.*, 2015, **8**, 2464–2470.
- 443 M. Kulbak, D. Cahen and G. Hodes, *J. Phys. Chem. Lett.*, 2015, **6**, 2452–2456.
- 444 *Research Cell Efficiency Records (NREL)*, <http://www.nrel.gov/ncpv/>, accessed: July 22, 2016.
- 445 E. J. Klem, D. D. MacNeil, P. W. Cyr, L. Levina and E. H. Sargent, *Appl. Phys. Lett.*, 2007, **90**, 183113.
- 446 J. M. Luther, M. Law, M. C. Beard, Q. Song, M. O. Reese, R. J. Ellingson and A. J. Nozik, *Nano Lett.*, 2008, **8**, 3488–3492.
- 447 W. Ma, J. M. Luther, H. Zheng, Y. Wu and A. P. Alivisatos, *Nano Lett.*, 2009, **9**, 1699–1703.
- 448 R. Debnath, J. Tang, D. A. Barkhouse, X. Wang, A. G. Pattantyus-Abraham, L. Brzozowski, L. Levina and E. H. Sargent, *J. Am. Chem. Soc.*, 2010, **132**, 5952–5953.
- 449 W. Ma, S. L. Swisher, T. Ewers, J. Engel, V. E. Ferry, H. A. Atwater and A. P. Alivisatos, *ACS Nano*, 2011, **5**, 8140–8147.
- 450 A. H. Ip, S. M. Thon, S. Hoogland, O. Voznyy, D. Zhitomirsky, R. Debnath, L. Levina, L. R. Rollny, G. H. Carey and A. Fischer, *et al.*, *Nat. Nanotechnol.*, 2012, **7**, 577–582.
- 451 Z. Ning, D. Zhitomirsky, V. Adinolfi, B. Sutherland, J. Xu, O. Voznyy, P. Maraghechi, X. Lan, S. Hoogland and Y. Ren, *et al.*, *Adv. Mater.*, 2013, **25**, 1719–1723.
- 452 E. T. McClure, M. R. Ball, W. Windl and P. M. Woodward, *Chem. Mater.*, 2016, **28**, 1348–1354.
- 453 M. R. Filip, S. Hillman, A. A. Haghighirad, H. J. Snaith and F. Giustino, *J. Phys. Chem. Lett.*, 2016, **7**, 2579–2585.
- 454 F. Wei, Z. Deng, S. Sun, F. Xie, G. Kieslich, D. M. Evans, M. A. Carpenter, P. D. Bristowe and A. K. Cheetham, *Mater. Horiz.*, 2016, **3**, 328–332.
- 455 Z. Deng, F. Wei, S. Sun, G. Kieslich, A. K. Cheetham and P. D. Bristowe, *J. Mater. Chem. A*, 2016, **4**, 12025–12029.
- 456 Y.-Y. Sun, J. Shi, J. Lian, W. Gao, M. L. Agiorgousis, P. Zhang and S. Zhang, *Nanoscale*, 2016, **8**, 6284–6289.
- 457 S. Wang, D. B. Mitzi, G. A. Landrum, H. Genin and R. Hoffmann, *J. Am. Chem. Soc.*, 1997, **119**, 724–732.
- 458 D. B. Mitzi, *Inorg. Chem.*, 1996, **35**, 7614–7619.
- 459 D. B. Mitzi and P. Brock, *Inorg. Chem.*, 2001, **40**, 2096–2104.
- 460 K. R. Maxcy, R. D. Willett, D. B. Mitzi and A. Afzali, *Acta Crystallogr., Sect. E: Struct. Rep. Online*, 2003, **59**, m364–m366.
- 461 W.-X. Chai, J. Lin, L. Song, L.-S. Qin, H.-S. Shi, J.-Y. Guo and K.-Y. Shu, *Solid State Sci.*, 2012, **14**, 1226–1232.
- 462 S. A. Adonin, I. D. Gorokh, D. G. Samsonenko, M. N. Sokolov and V. P. Fedin, *Chem. Commun.*, 2016, **52**, 5061–5063.
- 463 S. Sun, S. Tominaka, J.-H. Lee, F. Xie, P. D. Bristowe and A. K. Cheetham, *APL Mater.*, 2016, **4**, 031101.
- 464 N. A. Yelovik, A. V. Mironov, M. A. Bykov, A. N. Kuznetsov, A. V. Grigorieva, Z. Wei, E. V. Dikarev and A. V. Shevelkov, *Inorg. Chem.*, 2016, **55**, 4132–4140.
- 465 C. Silvestru, H. J. Breunig and H. Althaus, *Chem. Rev.*, 1999, **99**, 3277–3328.
- 466 D. B. Mitzi, in *Synthesis, Structure, and Properties of Organic-Inorganic Perovskites and Related Materials*, ed. K. D. Karlin, John Wiley & Sons, Inc., Hoboken, NJ, USA, 2007, vol. 48, pp. 1–121.
- 467 M. A. Green, K. Emery, Y. Hishikawa, W. Warta and E. D. Dunlop, *Prog. Photovolt: Res. Appl.*, 2016, **24**, 905–913.

